A compressible two-fluid multiphase model for CO2 leakage through a wellbore

Musivand Arzanfudi, M; Al-Khoury, RIN

DOI
10.1002/fld.3990

Publication date
2015

Document Version
Accepted author manuscript

Published in
International Journal for Numerical Methods in Fluids

Citation (APA)
Musivand Arzanfudi, M., & Al-Khoury, RIN. (2015). A compressible two-fluid multiphase model for CO2 leakage through a wellbore. *International Journal for Numerical Methods in Fluids*, *77*(8), 477-507. https://doi.org/10.1002/fld.3990

A compressible two-fluid multiphase model for CO_2 leakage through a wellbore

Mehdi Musivand Arzanfudi [*] , Rafid Al-Khoury

Faculty of Civil Engineering and Geosciences, Delft University of Technology, P.O. Box 5048, 2600 GA Delft, The Netherlands

Abstract

This paper introduces an effectively mesh-independent and computationally efficient model for CO_2 leakage through wellbores. A one dimensional compressible two-fluid domain, representing a homogeneous air gas and a multiphase CO_2 with a jump at the interface between them, is modeled.

The physical domain is modeled using the drift-flux model, and the governing equations are solved using a mixed finite element discretization scheme. The standard Galerkin finite element method, the partition of unity method and the level-set method are integrated to solve the problem. All important physical phenomena and processes occurring along the wellbore path, including fluid dynamics, buoyancy, phase change, compressibility, thermal interaction, wall friction and slip between phases, together with the jump in density and enthalpy between air and CO_2, are considered. Two numerical examples illustrating the computational capability and efficiency of the model are presented.

Keywords: CO_2 sequestration, drift-flux model, computational fluid dynamics, partition of unity, level set

1 Introduction

CO_2 geo-sequestration is currently utilized as a means to mitigate CO_2 emission into the earth atmosphere in an attempt to reduce the likely greenhouse effect. Selection of an appropriate geological formation for CO_2 sequestration requires a good estimate of the amount of leakage that might take place in time. Leakage of CO_2 to the ground surface or upper layers containing ground water is hazardous and considered as one of the major concerns of applying this technology. It is therefore vital to develop computational tools capable of modelling the leakage processes and phenomena. Two kinds of CO_2 leakage can be identified: leakage via heterogeneous layered domains, for which the theory of

[*] Corresponding author: Mehdi Musivand Arzanfudi

Faculty of Civil Engineering and Geosciences, Delft University of Technology, P.O. Box 5048, 2600 GA Delft, The Netherlands. Tel.: +31 (0)15 27 88216

E-mail: M.MusivandArzanfudi@tudelft.nl

multiphase flow in porous medium domains is applicable; and leakage via faults and abandoned wells, for which the theory of fluid dynamics is applicable. The focus in this paper is placed on leakage via abandoned wellbores.

The physical processes of CO_2 leakage via a wellbore and the involved flow mechanisms are rather complicated. They involve movement of multiple fluids comprising multiple phases which can be dispersed, mixed and have no distinct interfaces between them. Several coupled mechanisms including buoyancy, heat transfer, phase change, compressibility, wall friction and slip between phases are involved. Computational modelling of such a physical combination occurring in a wellbore, hundreds of meters long, is challenging.

Modeling fluid flow in wellbores has been a field of wide interest in oil and gas industry. A detailed review of the relevant physical processes and mathematical formulations can be found in Brill and Mukherjee [1] and Hasan *et al.* [2]. A review on the earlier wellbore models and codes can be found in Freeston and Hadgu [3] and Probst *et al.* [4]. An excellent overview of transport phenomena in multiphase systems is given by Faghri and Zhang [5].

As the computational modeling of fluid flow is challenging and time and capacity demanding, different models deal with different aspects of the involved processes and geometry. Some treat CO_2 as a single phase and others treat it as a mixture; while many models simulate leakage in the wells only, and others are coupled with the reservoir. Some consider steady-state flow with no phase change, whereas several others consider transient flow with phase change. Stone *et al.* [6] proposed a finite volume model for coupled wellbore-reservoir transient two-fluid (oil-water), three-phase flow in the wellbore with phase change of water only (water/steam). Hadgu *et al.* [7] modeled transient two-fluid flow in a coupled wellbore-reservoir domain without phase change, using the coupled WFSA-TOUGH code. Livescu *et al.* [8] introduced a finite volume model for coupled wellbore-reservoir transient three-fluid, three-phase flow with phase change for oil and gas applications. Hasan and Kabir [9] presented a steady-state model for single-fluid (water) flow with phase change (water/steam). Recently, Pan and Oldenburg [10] developed a transient finite volume model for coupled wellbore-reservoir for compressed air energy storage applications that include a two-fluid domain consisting of water and air but no phase change.

Regarding CO_2 flow in a wellbore, Cronshaw and Bolling [11] developed a finite volume numerical model for transient two-fluid (CO_2-water), three-phase flow in the wellbore with phase change of CO_2 only. Lu and Connell [12] and Lindeberg [13] introduced models based on Runge–Kutta finite difference method to simulate steady-state two-phase, single-fluid flow of CO_2 with phase change in the wellbore. Paterson *et al.* [14] modeled a transient two-phase, single-fluid flow of CO_2 with phase change in the wellbore. Pan *et al.* [15] presented a finite volume model for transient flow in wellbores of two-fluid (CO_2-brine) with phase change of CO_2 only. Remoroza *et al.* [16] utilized TOUGH2 to study the coupled wellbore-reservoir steady-state two-fluid flow (CO_2 and water) with no phase change for geothermal heat flow applications.

In these models, while providing very useful basis for developing computational tools for fluid flow in wellbores, the focus is placed on modeling the physical processes, rather than the numerical solutions. Mostly, standard numerical discretization schemes are utilized. This normally requires the use of excessively fine meshes (grids) with adaptive meshing, or some other appropriate approaches. As a consequence, these models suffer from two main shortcomings: 1. computational inefficiency, and 2. mesh size dependency. This paper intensively addresses a solution to these two issues.
The objective of this work is to develop an accurate, mesh-independent and computationally efficient transient model for CO_2 leakage through wellbores. A detailed modeling approach is given hereafter.

2 Modeling approach

Deriving an accurate, mesh-independent and computationally efficient transient model for CO_2 leakage from a geo-sequestration site via an abandoned wellbore requires a well-designed formulation of the mathematical model and the numerical model.

Regarding the mathematical model, it is apparent that the model should take into consideration all important physical phenomena and processes occurring along the wellbore. Fluid dynamics, buoyancy, phase change, compressibility, thermal interactions, wall friction, slip between phases, together with all relevant thermodynamic relationships must be considered. Initially, the wellbore is filled with air and the CO_2 in the reservoir is, most probably, in a supercritical state. Upon leakage, the CO_2 changes phase and starts displacing the air. This gives rise to having two fluids in the domain: air and CO_2. The air is a homogeneous gas, and the CO_2 is a multiphase fluid constituting supercritical liquid, liquid and gas, which are, in general, dispersed, mixed and having no distinct interfaces. The physical processes of such a domain are governed by the conservation laws of transport of mass, momentum and energy given by the Navier-Stokes equations. As the size of the engineering system that we are dealing with is huge and the CO_2 phases are dispersed and mixed, relying on an averaging approach is indispensable. Here, we model the air and the CO_2 as two separate fluids. The air is modeled as a homogenous gas, and the CO_2 is modeled as a homogeneous mixture. The jump condition at the interface between the air and the CO_2 is considered. We utilize the one-dimensional drift-flux model to simulate the transport of air and CO_2 in the wellbore. This model adopts the area-averaged approach, where detailed analysis of the local behavior of the involved phases are averaged over the cross-sectional area of the wellbore. Important aspects of fluid dynamics such as the inertia force, buoyancy, wall friction, drift velocity, flow profile are considered in the drift-flux model.

To model two fluids, two sets of governing equations representing the two fluids are needed, together with a constraint condition at the interface between them. In literature, however, many models utilized for CO_2 flow in a wellbore, or similar applications, consider single phase with no phase change. The primary state variables usually utilized in such models are velocity, pressure and temperature. For a single phase, such primary variables are sufficient, as the variation of enthalpy is

directly related to the variations of temperature and pressure. However, for a multiphase, the fluid temperature is not directly related to the enthalpy, and additional constitutive equations relating the variation of enthalpy to the variations of pressure, temperature, entropy and molar fraction are necessary (see Lu and Connell [12]).

Here, we utilize a set of drift-flux model equations to represent the two fluids, but impose a jump at the interface between them. This necessitates adopting the mass density as a primary state variable instead of the temperature to clearly distinguish between the two fluids. The set of the primary state variables in this paper is thus: velocity, pressure and density. In such a set, there is a fundamental thermodynamic relationship relating the fluid mass density to the gas/liquid volume fraction, that allows for a distinct separation between the liquid and gas phases, and avoids the additional constitutive relationships mentioned above. However, this should be supplemented with a proper numerical scheme capable of modeling the jump between the two fluids.

Regarding the numerical model, it is obvious that the model should take into consideration the local and global conservative nature of the system and its nonlinear hyperbolic characteristics. Using standard numerical discretization methods such as the finite difference, the finite volume or the finite element necessitate excessively fine grids and small time steps. Therefore, in order to obtain a computationally efficient model, adopting an advanced discretization procedure is indispensable. Here, we adopt a mixed discretization scheme. In this scheme, state variables exhibiting different physical nature are treated using different numerical discretization techniques. Techniques such as the standard Galerkin finite element method (SG), the partition of unity finite element method (PUM), and the level-set method (LS) are integrated in a single numerical scheme. SG is utilized to discretize the diffusive dominant field equations, and PUM, within the framework of the extended finite element method (XFEM), together with LS are utilized to discretize the advective dominant field equations. The level-set method is employed to trace and locate the CO_2 front, and the extended finite element method is employed to model the associated jump in the mass density field. The use of LS and XFEM for the advective field leads to a globally and locally conservative discretization, giving a stable and effectively mesh-independent scheme. The proposed mixed discretization scheme differs from the well-known mixed FEM such that in the mixed FEM, different state variables are utilized but adopt a single discretization technique; whereas in the mixed discretization scheme, we utilize different state variables and adopt different discretization techniques, depending on the physical nature of the state variable and the associated balance equations.

Compressible fluid dynamic equations inevitably involve acoustic waves. Numerically, this requires fine grids and small time steps. However, for CO_2 leakage in a wellbore, the time scale of interest is dominated by the time scale of the fluid advection, and hence, the acoustic waves pose no significance on the analysis. Therefore it is desirable to remove the acoustic wave from the system of equations. This is done by decoupling the pressure term of the balance momentum equation from the mass and energy equations.

3 Governing equations

The governing equations of the drift-flux model are described in many literature, including Shi *et al.* [17], Ishii and Hibiki [18] and Pan and Oldenburg [10]. Here, a listing of the governing equations of this model and its associated thermodynamic and engineering constitutive relationships is given. We utilize a set of governing equations to describe both, the air and the CO_2, but impose a jump at the interface between them. The fluids are allowed to exist at any state or mixture composition, depending on their thermodynamic conditions along the wellbore. However, no mass exchange at the interface is allowed. This assumption is justified because CO_2 leakage via a wellbore is advection-dominant and the rate of dissolution and diffusion between the two fluids is negligible. This inevitably entails that the fluids velocities and pressures at the interface are continuous, but discontinuous in the their mass density and enthalpy, giving:

$$\begin{aligned} &v_{\mathrm{co}_2} = v_{\mathrm{air}} \\ &p_{\mathrm{co}_2} = p_{\mathrm{air}} \qquad \text{at}\ \Gamma_d \\ &[\![\rho_m]\!] = \rho_{\mathrm{co}_2} - \rho_{\mathrm{air}} \\ &[\![h_m]\!] = h_{\mathrm{co}_2} - h_{\mathrm{air}} \end{aligned} \tag{1}$$

3.1 Drift-flux balance equations with discontinuity

Based on the drift-flux model, the balance equations of fluid mixture flow in one dimension with a jump condition at the interface between two separate fluids (air and CO_2) can be described as

Mass balance

$$\frac{\partial \rho_m}{\partial t} + \frac{\partial}{\partial z}(\rho_m v_m) + [\![\rho_m]\!] v_m \cdot n\,\delta(z - z_d) = 0 \tag{2}$$

Momentum balance

$$\frac{\partial}{\partial t}(\rho_m v_m) + \frac{\partial}{\partial z}\left(\rho_m v_m^2 + \gamma\right) + [\![\rho_m]\!] v_m^2 \cdot n\,\delta(z - z_d) = -\frac{\partial p}{\partial z} - \frac{f\,\rho_m |v_m| v_m}{4 r_i} - \rho_m g \sin\theta \tag{3}$$

Energy balance

$$\begin{aligned} &\frac{\partial}{\partial t}\left[\rho_m\left(h_m + \frac{1}{2}v_m^2\right) - p\right] + \frac{\partial}{\partial z}\left[\rho_m v_m\left(h_m + \frac{v_m^2}{2}\right)\right] \\ &\quad + [\![\rho_m]\!] v_m \left([\![h_m]\!] + \frac{v_m^2}{2}\right) \cdot n\,\delta(z - z_d) = \rho_m v_m g \sin\theta - \frac{Q}{\pi r_i^2} \end{aligned} \tag{4}$$

where δ is the Dirac delta function (unit= m^{-1}), z_d is the coordinate of interface between CO_2 and air, shown in Fig. 1, n is the unit normal vector, r_i is the inner radius of the wellbore, ρ_m is the mixture density, v_m is the mixture velocity, p is the pressure, f is the wall friction coefficient, g is

the gravitational constant, θ is the inclination angle of the well, h_m is the specific enthalpy of the mixture, Q is the heat exchange between the well and its surrounding formation, and γ describes the slip between two phases. The definitions of the drift flux model parameters are listed in Appendix A.

Fig. 1 Definitions of domains, interface, coordinate and unit normal vector to the boundary

3.2 Constitutive equations

A comprehensive treatment of the CO_2 constitutive equations is given in Musivand Arzanfudi and Al-Khoury [19]. The relevant constitutive equations for the CO_2, together with those for air, are given in Appendix B.

3.3 Initial and boundary conditions

Initially, the primary state variables might be described as

$$G(z,0)=G_0(z) \quad \text{at} \quad t=0 \tag{5}$$

where G can be v_m, p, or ρ_m.

The Dirichlet boundary conditions might be described as

$$G(t)=\hat{G}(t) \quad \text{on} \ \Gamma_u \tag{6}$$

in which Γ_u is the Dirichlet boundary.

The Neumann boundary conditions are defined as

$$\begin{aligned} \hat{q}_\rho &= (\hat{\rho}_m \hat{v}_m)\cdot n \\ \hat{q}_v &= (\hat{\rho}_m \hat{v}_m^2 + \hat{\gamma})\cdot n \qquad \text{on}\ \Gamma_q \\ \hat{q}_e &= \left[\hat{\rho}_m \hat{v}_m \left(\hat{h}_m + \frac{\hat{v}_m^2}{2}\right)\right]\cdot n \end{aligned} \tag{7}$$

where Γ_q is the Neumann boundary, and the subscripts ρ, v and e refer to mass, momentum and energy, respectively.

At an outflow boundary, the Neumann boundary conditions are defined as

$$\begin{aligned} q_\rho &= (\rho_m v_m)\cdot n \\ q_v &= (\rho_m v_m^2 + \gamma)\cdot n \qquad \text{on}\ \Gamma_o \\ q_e &= \left[\rho_m v_m \left(h_m + \frac{v_m^2}{2}\right)\right]\cdot n \end{aligned} \tag{8}$$

where Γ_o is the outflow boundary. Note that the primary state variables at this boundary are not known and have to be calculated. Otherwise, this boundary becomes by definition close, or have to be assigned a typical Dirichlet or Neumann boundary conditions. As it will be shown later, the discretization of this kind of boundary conditions will add up terms to the finite element matrices, including the left-hand side.

4 Modeling the discontinuity between air and CO_2

At the front of the CO_2 plume, a discontinuity in the density field, together with other thermodynamic properties differentiating air from CO_2, exists. This discontinuity is traced using the level-set method.

4.1 Tracing the front: level-set method

The level-set method is a numerical technique usually utilized to trace a moving interface, Γ_d, between two zones, for instance, Ω^+ and Ω^-. A level-set function is defined as a signed distance function, $\phi(z)$, which is positive in Ω^+, negative in Ω^-, and zero at the interface between them. For a one-dimensional domain, it can be described as

$$\phi(z)=\begin{cases} |z-z_d| & z\in\Omega^+ \\ -|z-z_d| & z\in\Omega^- \end{cases} \qquad \phi(z)\in\Re,\ z\in\Omega \tag{9}$$

where z_d is the coordinate of the interface. The sign indicates different domains, and the magnitude represents the distance to the interface. The level-set function is advected by a field motion equation of the form

$$\frac{\partial\phi}{\partial t}+v\frac{d\phi}{dz}=0 \tag{10}$$

where *v* represents the interface (front) velocity, taken here as the average of the two fluids velocities at the vicinity of the interface.

4.2 Thermodynamic properties

The thermodynamic properties of the two fluids exhibit a jump at the interface between them. For instance, the temperature can be calculated as a function of pressure and mixture density as

$$T\left(z,p,\rho_m\right)=\begin{cases} T_{\mathrm{co}_2}\left(p,\rho_m\right) & z\in\Omega^+ \\ T_{\mathrm{air}}\left(p,\rho_m\right) & z\in\Omega^- \end{cases} \tag{11}$$

where T_{co_2} is the CO_2 temperature in Ω^+ zone, and T_{air} is the air temperature in Ω^- zone. In terms of the level-set function, Eq. (11) can be described as

$$T(\phi, p, \rho_m) = \begin{cases} T_{\mathrm{co}_2}(p, \rho_m) & \phi > 0 \\ T_{\mathrm{air}}(p, \rho_m) & \phi \le 0 \end{cases} \tag{12}$$

This can be equivalently written as

$$T(\phi, p, \rho_m) = H(\phi) T_{\mathrm{co}_2}(p, \rho_m) + (1 - H(\phi)) T_{\mathrm{air}}(p, \rho_m) \tag{13}$$

where $H(\phi)$ is the Heaviside function, that reads

$$H(\phi) = \begin{cases} 1 & \phi > 0 \\ 0 & \phi \le 0 \end{cases} \tag{14}$$

Similar equations can be derived for the enthalpy, h_m, gas volume fraction, f_G, gas density, ρ_G, and liquid density, ρ_L.

5 Acoustic filtration

The fully compressible fluid flow equations given above are not exactly suited to the type of fluid flow in wellbores because of the inevitable generation of acoustic waves. The mean velocity flow of the CO_2 plume is much slower than that of the acoustic wave. Therefore, it is useful to filter out the unwanted acoustic modes. These modes can be filtered out by decoupling the pressure in the momentum equation from that arising from the density-temperature-pressure equations of state.

An early work in this field was introduced by Rehm and Baum [20], for inviscid flow; and Paolucci [21], for viscous flow. An in-depth analysis of this problem is given by Principe and Codina [22] and Reddy and Gartling [23].

The general approach is that the fluid pressure is decomposed into two terms: a spatially uniform, time-dependent background (thermodynamic) pressure $p_0(t)$; and a dynamical (mechanical) pressure, $p'(z,t)$; such that

$$p(z,t) = p_0(t) + p'(z,t) \tag{15}$$

The background pressure, $p_0(t)$, is utilized in the thermodynamic properties formulations, e.g. Eq. (13), such that

$$T(\phi, p_0, \rho_m) = H(\phi) T^c(p_0, \rho_m) + (1 - H(\phi)) T^a(p_0, \rho_m) \tag{16}$$

Other properties follow suite.

The dynamical pressure $p'(z,t)$ is utilized instead of the total pressure, p, which appears on the right-hand side of the momentum balance equations, Eq. (3).

The common practice of assuming $p_0(t)$ as spatially uniform can be in many cases realistic, especially those dealing with relatively small geometry constituting fluids with an insignificant pressure variation. However, for a CO_2 leakage case, which involves long wellbores with a huge pressure variation along its length, this assumption is not realistic. To circumvent this, we assume this pressure to have a linear variation between the pressure at the bottom boundary and that at the top boundary of the wellbore. This is done at every time step, giving

$$p(z,t) = p_0(z,t) + p'(z,t) \tag{17}$$

Following this, and since the background pressure is a function of space as well, the original momentum balance equation, Eq. (3), can be utilized. The use of acoustic filtration allows for using larger time step sizes while preserving the accuracy of the results [23], which will obviously result in a more efficient computational model.

6 Mixed discretization finite element scheme (PUM-SG)

The governing drift-flux equations, together with the initial and boundary conditions, form an initial and boundary value problem that is dynamic, advective, nonlinear and involves a jump condition. Solving such a problem using standard finite element procedures entails utilization of excessively fine and adaptive meshes and small time steps, but nevertheless, the model can be unstable and the results are very likely mesh-dependent. Above all, standard finite element discretization procedure is not locally convergent, a feature necessary to model the jump condition at the interface between the two fluids. To tackle this, we solve the problem using a mixed finite element discretization scheme. This scheme entails solving different balance equations using different discretization schemes, which are tailored to accurately describe the nature of the involved primary state variables v_m, p, and ρ_m. The discontinuity at the interface is modeled using the level-set method to trace the interface; and the partition of unity to discretize the mass density.

6.1 Level-set discretization

Applying the weighted residual finite element discretization procedure to Eq. (10) gives

$$\int_\Omega w \frac{\partial \phi}{\partial t} d\Omega + \int_\Omega w v \frac{d\phi}{dz} d\Omega = 0 \tag{18}$$

Approximating ϕ as $\phi = \mathbf{N}(z)\mathbf{\Phi}(t)$, with $\mathbf{N}(z)$ a vector of shape functions and $\mathbf{\Phi}(t)$ a vector of nodal values of the level-set function at time t, and assuming $w = \mathbf{N}$ yields

$$\int_\Omega \mathbf{N}^T \mathbf{N} \frac{\partial \mathbf{\Phi}}{\partial t} d\Omega + \int_\Omega \mathbf{N}^T v \frac{d\mathbf{N}}{dz} \mathbf{\Phi}\, d\Omega = 0 \tag{19}$$

Utilizing the level-set method to trace a moving front requires re-distancing (re-initialization) at every time step. This is necessary because otherwise the distance property of the level-set function is no longer maintained after advection. We utilize the direct distancing approach proposed by Cho *et al.* [24] for this purpose. In this approach, the re-distancing is performed by geometrical updating of the advective front instead of solving a re-initialization equation.

6.2 PUM-SG formulation

The standard Galerkin finite element method (SG) and the partition of unity method (PUM), within the framework of the extended finite element method, are integrated to discretize the problem. The first is, in general, accurate and computationally efficient for solving continuous problems, and the second is accurate and effective in solving discontinuous problems.

As stated above, the mixture velocity and pressure are continuous at the interface between CO_2 and air, and thus SG suffices, entailing

$$v_m(z,t) = \sum_{i \in I} N_i(z) v_{mi}(t) = \mathbf{N}(z)\mathbf{v}_m(t) \tag{20}$$

$$p = \sum_{i \in I} N_i(z)\, p_i(t) = \mathbf{N}(z)\mathbf{p}(t) \tag{21}$$

in which I is the set of all nodes in the domain, $N_i(z)$ is the shape function of node i, $v_{mi}(t)$ and $p_i(t)$ are the nodal values of the mixture velocity and pressure for node i, respectively, and $\mathbf{N}(z)$, $\mathbf{v}_m(t)$, and $\mathbf{p}(t)$ are the associated nodal vectors.

On the other hand, the mixture mass density is discontinuous at the interface between CO_2 and air, and for this PUM suffices, entailing

$$\begin{aligned} \rho_m(z,t) &= \sum_{i \in I} N_i(z)\rho_{mi}(t) + \sum_{i \in I^*} N_i^{eh}(z)\,\tilde{\rho}_{mi}(t) \\ &= \mathbf{N}(z)\boldsymbol{\rho}_m(t) + \mathbf{N}^{eh}(z)\tilde{\boldsymbol{\rho}}_m(t) \end{aligned} \tag{22}$$

where I^* is the subset of enriched nodes, $\rho_{mi}(t)$ and $\tilde{\rho}_{mi}(t)$ are the conventional and additional (extended) nodal values of the mixture density at node i, and $N_i^{eh}(z)$ is an enriched shape function at node i, and $\boldsymbol{\rho}_m(t)$, $\tilde{\boldsymbol{\rho}}_m(t)$ and $\mathbf{N}^{eh}(z)$ are the associated nodal vectors. $N_i^{eh}(z)$ is defined as

$$N_i^{eh}(z) = N_i(z)\psi_i(\phi) \tag{23}$$

in which $\psi_i(\phi)$ is the shifted enrichment function [25] at node i, defined as

$$\psi_i(\phi) = H(\phi) - H(\phi_i) \tag{24}$$

where ϕ_i is the value of level-set function at node i. Using the shifted PUM leads to the existence of a non-zero enriched shape function over both sides of the discontinuity. Consequently, the density of each fluid across the discontinuity is calculated as

$$\begin{aligned}\rho_{\mathrm{co}_2}\left(z_d,t\right)&=\mathbf{N}\left(z_d\right)\boldsymbol{\rho}_m\left(t\right)+\mathbf{N}^{eh+}\left(z_d\right)\tilde{\boldsymbol{\rho}}_m\left(t\right)\\ \rho_{\mathrm{air}}\left(z_d,t\right)&=\mathbf{N}\left(z_d\right)\boldsymbol{\rho}_m\left(t\right)+\mathbf{N}^{eh-}\left(z_d\right)\tilde{\boldsymbol{\rho}}_m\left(t\right)\end{aligned} \tag{25}$$

in which $\mathbf{N}^{eh+}$ and $\mathbf{N}^{eh-}$ are the enriched shape functions at the neighborhood of the discontinuity on Ω^+ and Ω^-, respectively. Note that we utilized the shifted enrichment approximation because the conventional un-shifted PUM does not, in general, have the Kronecker-δ property of the standard FEM, rendering the imposition of essential boundary conditions difficult. A comprehensive treatment of this issue is given by Fries and Belytschko [26].

Using the weighted residual method, the finite element formulation of the governing equations; Eqs. (2), (3) and (4); can be described as

Mass balance

$$\int_\Omega w\frac{\partial\rho_m}{\partial t}d\Omega+\int_\Omega w\frac{\partial}{\partial z}\left(\rho_m v_m\right)d\Omega+\int_{\Gamma_d} w\left[\!\left[\rho_m\right]\!\right]v_m\cdot n\,d\Gamma=0 \tag{26}$$

Momentum balance

$$\begin{aligned}&\int_\Omega w'\frac{\partial}{\partial t}\left(\rho_m v_m\right)d\Omega+\int_\Omega w'\frac{\partial}{\partial z}\left(\rho_m v_m^2+\gamma\right)d\Omega+\int_{\Gamma_d} w'\left[\!\left[\rho_m\right]\!\right]v_m^2\cdot n\,d\Gamma\\ &\quad=-\int_\Omega w'\frac{\partial p}{\partial z}d\Omega-\int_\Omega w'\frac{f\rho_m\left|v_m\right|v_m}{4r_i}d\Omega-\int_\Omega w'\rho_m g\sin\theta d\Omega\end{aligned} \tag{27}$$

Energy balance

$$\begin{aligned}&\int_\Omega w''\frac{\partial}{\partial t}\left[\rho_m\left(h_m+\frac{1}{2}v_m^2\right)-p\right]d\Omega+\int_\Omega w''\frac{\partial}{\partial z}\left[\rho_m v_m\left(h_m+\frac{v_m^2}{2}\right)\right]d\Omega\\ &\quad+\int_{\Gamma_d} w''\left[\!\left[\rho_m\right]\!\right]v_m\left(\left[\!\left[h_m\right]\!\right]+\frac{v_m^2}{2}\right)\cdot n\,d\Gamma=\int_\Omega w''\rho_m v_m g\sin\theta d\Omega-\int_\Omega w''\frac{Q}{\pi r_i^2}d\Omega\end{aligned} \tag{28}$$

in which w, w' and w'' are the weighting functions of the mass, momentum and energy balance equations respectively.

As the discontinuity occurs in one primary state variable, only one balance equation is needed to be partitioned. For this, we chose the energy balance equation since its jump term contains the specific enthalpy term, which is a function of density, and accordingly exhibiting a discontinuity at the interface between air and CO_2. Thus, for the mass and momentum balance equations, a continuous weighting function is utilized; whereas for the energy balance equation, a discontinuous weighting function is utilized, i.e.

$$w = w' = \mathbf{N} \tag{29}$$

$$w'' = \mathbf{N} + \mathbf{N}^{eh} \tag{30}$$

where the dependency on the spatial coordinates are ignored for simplicity of notation.

Substituting Eq. (29) into Eqs. (26) and (27), and applying Green's theorem, yields

Mass balance

$$\begin{aligned}&\int_\Omega \mathbf{N}^T \mathbf{N}\dot{\boldsymbol{\rho}}_m d\Omega + \int_\Omega \mathbf{N}^T \mathbf{N}^{eh}\dot{\tilde{\boldsymbol{\rho}}}_m d\Omega - \int_\Omega \mathbf{B}^T v_m \mathbf{N}\boldsymbol{\rho}_m d\Omega - \int_\Omega \mathbf{B}^T v_m \mathbf{N}^{eh}\tilde{\boldsymbol{\rho}}_m d\Omega \\ &\quad + \int_{\Gamma_q} \mathbf{N}^T \hat{q}_\rho d\Gamma + \int_{\Gamma_o} \mathbf{N}^T \left(\rho_m v_m\right)\cdot n\, d\Gamma + \int_{\Gamma_d} \mathbf{N}^T \left[\!\left[\rho_m\right]\!\right] v_m \cdot n\, d\Gamma = 0\end{aligned} \tag{31}$$

in which $\mathbf{B} = \partial\mathbf{N} / \partial z$.

Momentum balance

$$\begin{aligned}&\int_\Omega \mathbf{N}^T \left(v_m \mathbf{N}\dot{\boldsymbol{\rho}}_m + v_m \mathbf{N}^{eh}\dot{\tilde{\boldsymbol{\rho}}}_m + \rho_m \mathbf{N}\dot{\mathbf{v}}_m\right) d\Omega - \int_\Omega \mathbf{B}^T \left(\rho_m v_m \mathbf{N}\mathbf{v}_m + \gamma\right) d\Omega \\ &\quad + \int_{\Gamma_q} \mathbf{N}^T \hat{q}_v d\Gamma + \int_{\Gamma_o} \mathbf{N}^T \left(\rho_m v_m^2 + \gamma\right)\cdot n\, d\Gamma + \int_{\Gamma_d} \mathbf{N}^T \left[\!\left[\rho_m\right]\!\right] v_m^2 \cdot n\, d\Gamma \\ &\quad = -\int_\Omega \mathbf{N}^T \mathbf{B}\,\mathbf{p} d\Omega - \int_\Omega \mathbf{N}^T \frac{f\rho_m |v_m|}{4r_i} \mathbf{N}\mathbf{v}_m d\Omega - \int_\Omega \mathbf{N}^T \rho_m g \sin\theta\, d\Omega\end{aligned} \tag{32}$$

Substituting Eq. (30) into Eq. (28) and applying Green's theorem yields two equations: one representing a continuously weighted field and a discontinuously weighted field, as

Energy balance

continuously weighted:

$$\begin{aligned}&\int_\Omega \mathbf{N}^T \left[\left(h_m + \frac{1}{2}v_m^2\right)\mathbf{N}\dot{\boldsymbol{\rho}}_m + \left(h_m + \frac{1}{2}v_m^2\right)\mathbf{N}^{eh}\dot{\tilde{\boldsymbol{\rho}}}_m + \dot{h}_m \mathbf{N}\boldsymbol{\rho}_m + \dot{h}_m \mathbf{N}^{eh}\tilde{\boldsymbol{\rho}}_m + \rho_m v_m \mathbf{N}\dot{\mathbf{v}}_m - \mathbf{N}\dot{\mathbf{p}}\right] d\Omega \\ &\quad - \int_\Omega \mathbf{B}^T \left[\rho_m \left(h_m + \frac{v_m^2}{2}\right)\mathbf{N}\mathbf{v}_m\right] d\Omega + \int_{\Gamma_q} \mathbf{N}^T \hat{q}_e d\Gamma + \int_{\Gamma_o} \mathbf{N}^T \left[\rho_m v_m \left(h_m + \frac{v_m^2}{2}\right)\right]\cdot n\, d\Gamma \\ &\quad + \int_{\Gamma_d} \mathbf{N}^T \left[\!\left[\rho_m\right]\!\right] v_m \left(\left[\!\left[h_m\right]\!\right] + \frac{{v_m}^2}{2}\right)\cdot n\, d\Gamma = \int_\Omega \mathbf{N}^T \rho_m v_m g \sin\theta\, d\Omega - \int_\Omega \mathbf{N}^T \frac{Q}{\pi r_i^2} d\Omega\end{aligned} \tag{33}$$

discontinuously weighted:

$$\begin{aligned}&\int_\Omega \left(\mathbf{N}^{eh}\right)^T \left[\left(h_m + \frac{1}{2}v_m^2\right)\mathbf{N}\dot{\boldsymbol{\rho}}_m + \left(h_m + \frac{1}{2}v_m^2\right)\mathbf{N}^{eh}\dot{\tilde{\boldsymbol{\rho}}}_m + \dot{h}_m \mathbf{N}\boldsymbol{\rho}_m + \dot{h}_m \mathbf{N}^{eh}\tilde{\boldsymbol{\rho}}_m + \rho_m v_m \mathbf{N}\dot{\mathbf{v}}_m - \mathbf{N}\dot{\mathbf{p}}\right] d\Omega \\ &\quad - \int_\Omega \left(\mathbf{B}^{eh}\right)^T \left[\rho_m \left(h_m + \frac{v_m^2}{2}\right)\mathbf{N}\mathbf{v}_m\right] d\Omega + \int_{\Gamma_q} \left(\mathbf{N}^{eh}\right)^T \hat{q}_e d\Gamma + \int_{\Gamma_d} \left(\mathbf{N}^{eh}\right)^T \left[\!\left[\rho_m\right]\!\right] v_m \left(\left[\!\left[h_m\right]\!\right] + \frac{{v_m}^2}{2}\right)\cdot n\, d\Gamma \\ &\quad = \int_\Omega \left(\mathbf{N}^{eh}\right)^T \rho_m v_m g \sin\theta d\Omega - \int_\Omega \left(\mathbf{N}^{eh}\right)^T \frac{Q}{\pi r_i^2} d\Omega\end{aligned} \tag{34}$$

where $\mathbf{B}^{eh} = \partial \mathbf{N}^{eh} / \partial z$. Note that, unlike conventional PUM formulation, the integral of Eq. (34) is evaluated over $\Omega^+ \cup \Omega^- \equiv \Omega$ because the shifted enrichment function is non-zero over both sides of the discontinuity.

It is worth mentioning that the Neumann boundary conditions appearing in the finite element equations are a natural outcome of the Green's theorem. In other numerical schemes, such as the finite difference and finite volume, they have to be imposed a priori.

6.3 Linearization

The resulting weak formulations, Eqs. (31)-(34), represent a set of semi-discrete nonlinear equations, where the nonlinearity arises due to the constitutive relationships between the pressure and mixture density and other thermodynamic variables. Since the nonlinearity is due to scalar coefficients (i.e. v_m , ρ_m, h_m, etc.), and as the constitutive relationships are continuous (within a domain), it is convenient to linearize these equations using Taylor series expansions up to the first order (standard Newton-Raphson scheme).

The Taylor series expansion of the temperature T at the current iteration $r+1$, gives

$$T^{r+1} = T\left(p_0^r, \rho_m^r\right) + \frac{\partial T\left(p_0^r, \rho_m^r\right)}{\partial p_0} \delta p_0 + \frac{\partial T\left(p_0^r, \rho_m^r\right)}{\partial \rho_m} \delta \rho_m \tag{35}$$

or in a more concise form

$$T^{r+1} = T^r + \frac{\partial T^r}{\partial p_0} \delta p_0 + \frac{\partial T^r}{\partial \rho_m} \delta \rho_m \tag{36}$$

with

$$\begin{aligned} \delta p_0 &= p_0^{r+1} - p_0^r \\ \delta \rho_m &= \rho_m^{r+1} - \rho_m^r \end{aligned} \tag{37}$$

where the superscript r denotes the iteration number and the prefix δ denotes the increment of the state vector.

Since the background pressure is treated explicitly, as described in Section 5, its increment over a time step is set to zero, i.e. $\delta p_0 = 0$, and henceforth

$$T^{r+1} = T^r + \frac{\partial T^r}{\partial \rho_m} \delta \rho_m \tag{38}$$

Following this, the primary state variables and their time derivatives can be written as

$$\rho_m^{r+1} = \rho_m^r + \delta \rho_m \quad v_m^{r+1} = v_m^r + \delta v_m \quad p^{r+1} = p^r + \delta p \tag{39}$$

$$\dot{\rho}_m^{r+1} = \dot{\rho}_m^r + \delta \dot{\rho}_m \quad \dot{v}_m^{r+1} = \dot{v}_m^r + \delta \dot{v}_m \quad \dot{p}^{r+1} = \dot{p}^r + \delta \dot{p}$$

The other variables and their time derivatives can be written as follows:

Specific enthalpy

$$h_m^{r+1} = h_m\left(p_0^r, \rho_m^r\right) + \frac{\partial h_m\left(p_0^r, \rho_m^r\right)}{\partial p_0}\delta p_0 + \frac{\partial h_m\left(p_0^r, \rho_m^r\right)}{\partial \rho_m}\delta\rho_m \tag{40}$$

$$\dot{h}_m = \frac{\partial h_m\left(p_0, \rho_m\right)}{\partial p_0}\dot{p}_0 + \frac{\partial h_m\left(p_0, \rho_m\right)}{\partial \rho_m}\dot{\rho}_m \tag{41}$$

which after linearization, neglecting the dependency terms, reads

$$\begin{aligned}\dot{h}_m^{r+1} = &\left(\frac{\partial h_m^r}{\partial p_0} + \frac{\partial^2 h_m^r}{\partial p_0^2}\delta p_0 + \frac{\partial^2 h_m^r}{\partial p_0 \partial \rho_m}\delta\rho_m\right)\left(\dot{p}_0^r + \delta\dot{p}_0\right) \\ &+ \left(\frac{\partial h_m^r}{\partial \rho_m} + \frac{\partial^2 h_m^r}{\partial p_0 \partial \rho_m}\delta p_0 + \frac{\partial^2 h_m^r}{\partial \rho_m^2}\delta\rho_m\right)\left(\dot{\rho}_m^r + \delta\dot{\rho}_m\right)\end{aligned} \tag{42}$$

As for temperature, the increment due to the background pressure is eliminated, yeilding

$$\begin{aligned}h_m^{r+1} &= h_m^r + \frac{\partial h_m^r}{\partial \rho_m}\delta\rho_m^r \\ \dot{h}_m^{r+1} &= \left(\frac{\partial h_m^r}{\partial \rho_m} + \frac{\partial^2 h_m^r}{\partial \rho_m^2}\delta\rho_m\right)\left(\dot{\rho}_m^r + \delta\dot{\rho}_m\right)\end{aligned} \tag{43}$$

Slip term

$$\gamma^{r+1} = \gamma\left(v_m^r, p_0^r, \rho_m^r\right) + \frac{\partial\gamma\left(v_m^r, p_0^r, \rho_m^r\right)}{\partial v_m}\delta v_m + \frac{\partial\gamma\left(v_m^r, p_0^r, \rho_m^r\right)}{\partial p_0}\delta p_0 + \frac{\partial\gamma\left(v_m^r, p_0^r, \rho_m^r\right)}{\partial \rho_m}\delta\rho_m \tag{44}$$

Similarly, eliminating the background pressure, gives

$$\gamma^{r+1} = \gamma^r + \frac{\partial\gamma^r}{\partial v_m}\delta v_m + \frac{\partial\gamma^r}{\partial \rho_m}\delta\rho_m \tag{45}$$

Heat transfer

$$Q^{r+1} = Q\left(T\left(p_0^r, \rho_m^r\right)\right) + \frac{dQ}{dT}\delta T \tag{46}$$

$$Q^{r+1} = Q\left(T\left(p_0^r, \rho_m^r\right)\right) + \frac{dQ\left(T\left(p_0^r, \rho_m^r\right)\right)}{dT}\left(\frac{\partial T\left(p_0^r, \rho_m^r\right)}{\partial p_0}\delta p_0 + \frac{\partial T\left(p_0^r, \rho_m^r\right)}{\partial \rho_m}\delta\rho_m\right) \tag{47}$$

Eliminating the background pressure, gives

$$Q^{r+1} = Q^r + \frac{dQ^r}{dT}\frac{\partial T^r}{\partial \rho_m}\delta\rho_m \tag{48}$$

Reynolds number

$$\delta \mathrm{Re} = \frac{\partial \mathrm{Re}^r}{\partial v_m}\delta v_m + \frac{\partial \mathrm{Re}^r}{\partial p_0}\delta p_0 + \frac{\partial \mathrm{Re}^r}{\partial \rho_m}\delta \rho_m \tag{49}$$

Using Eq. (A.2), gives

$$\delta \mathrm{Re} = \frac{\rho_m^r \mathrm{sign}\left(v_m^r\right)(2r_i)}{\mu_m^r}\delta v_m - \frac{\rho_m^r \left|v_m^r\right|(2r_i)}{\left(\mu_m^r\right)^2}\frac{\partial \mu_m^r}{\partial p_0}\delta p_0 + \left(\frac{\left|v_m^r\right|(2r_i)}{\mu_m^r} - \frac{\rho_m^r \left|v_m^r\right|(2r_i)}{\left(\mu_m^r\right)^2}\frac{\partial \mu_m^r}{\partial \rho_m}\right)\delta \rho_m \tag{50}$$

Eliminating the background pressure, gives

$$\delta \mathrm{Re} = \frac{\rho_m^r \mathrm{sign}\left(v_m^r\right)(2r_i)}{\mu_m^r}\delta v_m + \left(\frac{\left|v_m^r\right|(2r_i)}{\mu_m^r} - \frac{\rho_m^r \left|v_m^r\right|(2r_i)}{\left(\mu_m^r\right)^2}\frac{\partial \mu_m^r}{\partial \rho_m}\right)\delta \rho_m \tag{51}$$

Wall friction

$$f^{r+1} = f^r + \frac{\partial f^r}{\partial \mathrm{Re}}\delta \mathrm{Re} \tag{52}$$

Using Eq. (51), gives

$$\begin{aligned} f^{r+1} = f^r &+ \frac{\rho_m^r \mathrm{sign}\left(v_m^r\right)(2r_i)}{\mu_m^r}\frac{\partial f^r}{\partial \mathrm{Re}}\delta v_m - \frac{\rho_m^r \left|v_m^r\right|(2r_i)}{\left(\mu_m^r\right)^2}\frac{\partial f^r}{\partial \mathrm{Re}}\frac{\partial \mu_m^r}{\partial p_0}\delta p_0 \\ &+ \left(\frac{\left|v_m^r\right|(2r_i)}{\mu_m^r} - \frac{\rho_m^r \left|v_m^r\right|(2r_i)}{\left(\mu_m^r\right)^2}\frac{\partial \mu_m^r}{\partial \rho_m}\right)\frac{\partial f^r}{\partial \mathrm{Re}}\delta \rho_m \end{aligned} \tag{53}$$

Eliminating the background pressure, gives

$$f^{r+1} = f^r + \frac{\rho_m^r \mathrm{sign}\left(v_m^r\right)(2r_i)}{\mu_m^r}\frac{\partial f^r}{\partial \mathrm{Re}}\delta v_m + \left(\frac{\left|v_m^r\right|(2r_i)}{\mu_m^r} - \frac{\rho_m^r \left|v_m^r\right|(2r_i)}{\left(\mu_m^r\right)^2}\frac{\partial \mu_m^r}{\partial \rho_m}\right)\frac{\partial f^r}{\partial \mathrm{Re}}\delta \rho_m \tag{54}$$

6.4 Finite element equations

Inserting Eqs. (38)-(54) into Eqs. (31)-(34) and using Eq. (1), after rearrangements, gives:

Mass field equations

$$\begin{aligned}
&\int_\Omega \mathbf{N}^T\mathbf{N}\dot{\boldsymbol{\rho}}_m^r d\Omega+\int_\Omega \mathbf{N}^T\mathbf{N}\delta\dot{\boldsymbol{\rho}}_m d\Omega+\int_\Omega \mathbf{N}^T\mathbf{N}^{eh}\dot{\tilde{\boldsymbol{\rho}}}_m^r d\Omega+\int_\Omega \mathbf{N}^T\mathbf{N}^{eh}\delta\dot{\tilde{\boldsymbol{\rho}}}_m d\Omega\\
&-\int_\Omega \mathbf{B}^T\rho_m^r\mathbf{N}\mathbf{v}_m^r d\Omega-\int_\Omega \mathbf{B}^T v_m^r\mathbf{N}\delta\boldsymbol{\rho}_m d\Omega-\int_\Omega \mathbf{B}^T v_m^r\mathbf{N}^{eh}\delta\tilde{\boldsymbol{\rho}}_m d\Omega-\int_\Omega \mathbf{B}^T\rho_m^r\mathbf{N}\delta\mathbf{v}_m d\Omega\\
&+\int_{\Gamma_d}\mathbf{N}^T\rho_{\mathrm{co}_2}^r\mathbf{N}\mathbf{v}_m^r\cdot n\,d\Gamma+\int_{\Gamma_d}\mathbf{N}^T\rho_{\mathrm{co}_2}^r\mathbf{N}\delta\mathbf{v}_m\cdot n\,d\Gamma+\int_{\Gamma_d}\mathbf{N}^T v_m^r\mathbf{N}\delta\boldsymbol{\rho}_m^r\cdot n\,d\Gamma\\
&+\int_{\Gamma_d}\mathbf{N}^T v_m^r\mathbf{N}^{eh+}\delta\tilde{\boldsymbol{\rho}}_m\cdot n\,d\Gamma-\int_{\Gamma_d}\mathbf{N}^T\rho_{\mathrm{air}}^r\mathbf{N}\mathbf{v}_m^r\cdot n\,d\Gamma-\int_{\Gamma_d}\mathbf{N}^T\rho_{\mathrm{air}}^r\mathbf{N}\delta\mathbf{v}_m\cdot n\,d\Gamma\\
&-\int_{\Gamma_d}\mathbf{N}^T v_m^r\mathbf{N}\delta\boldsymbol{\rho}_m\cdot n\,d\Gamma-\int_{\Gamma_d}\mathbf{N}^T v_m^r\mathbf{N}^{eh-}\delta\tilde{\boldsymbol{\rho}}_m\cdot n\,d\Gamma\\
&+\int_{\Gamma_o}\mathbf{N}^T\rho_m^r\mathbf{N}\mathbf{v}_m^r\cdot n\,d\Gamma+\int_{\Gamma_o}\mathbf{N}^T\rho_m^r\mathbf{N}\delta\mathbf{v}_m\cdot n\,d\Gamma+\int_{\Gamma_o}\mathbf{N}^T v_m^r\mathbf{N}\delta\boldsymbol{\rho}_m\cdot n\,d\Gamma\\
&+\int_{\Gamma_o}\mathbf{N}^T v_m^r\mathbf{N}^{eh}\delta\tilde{\boldsymbol{\rho}}_m\cdot n\,d\Gamma+\int_{\Gamma_q}\mathbf{N}^T\hat{q}_\rho\,d\Gamma=0
\end{aligned}\tag{55}$$

in which $\rho_{\mathrm{co}_2}^r$ and ρ_{air}^r are the CO_2 and air mass densities at the vicinity of the interface between them, known from the previous iteration, *r*.

Similar discretization can be made for the momentum and energy field equations, that upon putting them together in a concise form, leads to

Mass field equations

$$\mathbf{K}_{11}\delta\mathbf{v}_m+\mathbf{K}_{13}\delta\boldsymbol{\rho}_m+\mathbf{K}_{14}\delta\tilde{\boldsymbol{\rho}}_m+\mathbf{C}_{13}\delta\dot{\boldsymbol{\rho}}_m+\mathbf{C}_{14}\delta\dot{\tilde{\boldsymbol{\rho}}}_m=\mathbf{f}_1-\left(\mathbf{K}_{11}^0\mathbf{v}_m^r+\mathbf{C}_{13}^0\dot{\boldsymbol{\rho}}_m^r+\mathbf{C}_{14}^0\dot{\tilde{\boldsymbol{\rho}}}_m^r\right)\tag{56}$$

Momentum field equations

$$\begin{aligned}
&\mathbf{K}_{21}\delta\mathbf{v}_m+\mathbf{K}_{22}\delta\mathbf{p}\ +\mathbf{K}_{23}\delta\boldsymbol{\rho}_m+\mathbf{K}_{24}\delta\tilde{\boldsymbol{\rho}}_m+\mathbf{C}_{21}\delta\dot{\mathbf{v}}_m+\mathbf{C}_{23}\delta\dot{\boldsymbol{\rho}}_m+\mathbf{C}_{24}\delta\dot{\tilde{\boldsymbol{\rho}}}_m\\
&=\mathbf{f}_2-\left(\mathbf{K}_{21}^0\mathbf{v}_m^r+\mathbf{K}_{22}^0\mathbf{p}^r+\mathbf{K}_{23}^0\boldsymbol{\rho}_m^r+\mathbf{K}_{24}^0\tilde{\boldsymbol{\rho}}_m^r+\mathbf{C}_{21}^0\dot{\mathbf{v}}_m^r+\mathbf{C}_{23}^0\dot{\boldsymbol{\rho}}_m^r+\mathbf{C}_{24}^0\dot{\tilde{\boldsymbol{\rho}}}_m^r\right)
\end{aligned}\tag{57}$$

Energy field equations

$$\begin{aligned}
&\mathbf{K}_{31}\delta\mathbf{v}_m+\mathbf{K}_{33}\delta\boldsymbol{\rho}_m+\mathbf{K}_{34}\delta\tilde{\boldsymbol{\rho}}_m+\mathbf{C}_{31}\delta\dot{\mathbf{v}}_m+\mathbf{C}_{32}\delta\dot{\mathbf{p}}\ +\mathbf{C}_{33}\delta\dot{\boldsymbol{\rho}}_m+\mathbf{C}_{34}\delta\dot{\tilde{\boldsymbol{\rho}}}_m\\
&=\mathbf{f}_3-\left(\mathbf{K}_{31}^0\mathbf{v}_m^r+\mathbf{K}_{33}^0\boldsymbol{\rho}_m^r+\mathbf{K}_{34}^0\tilde{\boldsymbol{\rho}}_m^r+\mathbf{C}_{31}^0\dot{\mathbf{v}}_m^r+\mathbf{C}_{32}^0\dot{\mathbf{p}}^r+\mathbf{C}_{33}^0\dot{\boldsymbol{\rho}}_m^r+\mathbf{C}_{34}^0\dot{\tilde{\boldsymbol{\rho}}}_m^r\right)
\end{aligned}\tag{58}$$

$$\begin{aligned}
&\mathbf{K}_{41}\delta\mathbf{v}_m+\mathbf{K}_{43}\delta\boldsymbol{\rho}_m+\mathbf{K}_{44}\delta\tilde{\boldsymbol{\rho}}_m+\mathbf{C}_{41}\delta\dot{\mathbf{v}}_m+\mathbf{C}_{42}\delta\dot{\mathbf{p}}\ +\mathbf{C}_{43}\delta\dot{\boldsymbol{\rho}}_m+\mathbf{C}_{44}\delta\dot{\tilde{\boldsymbol{\rho}}}_m\\
&=\mathbf{f}_4-\left(\mathbf{K}_{41}^0\mathbf{v}_m^r+\mathbf{K}_{43}^0\boldsymbol{\rho}_m^r+\mathbf{K}_{44}^0\tilde{\boldsymbol{\rho}}_m^r+\mathbf{C}_{41}^0\dot{\mathbf{v}}_m^r+\mathbf{C}_{42}^0\dot{\mathbf{p}}^r+\mathbf{C}_{43}^0\dot{\boldsymbol{\rho}}_m^r+\mathbf{C}_{44}^0\dot{\tilde{\boldsymbol{\rho}}}_m^r\right)
\end{aligned}\tag{59}$$

In a matrix form, these equations can be described as

$$\begin{pmatrix} \mathbf{K}_{11} & 0 & \mathbf{K}_{13} & \mathbf{K}_{14} \\ \mathbf{K}_{21} & \mathbf{K}_{22} & \mathbf{K}_{23} & \mathbf{K}_{24} \\ \mathbf{K}_{31} & 0 & \mathbf{K}_{33} & \mathbf{K}_{34} \\ \mathbf{K}_{41} & 0 & \mathbf{K}_{43} & \mathbf{K}_{44} \end{pmatrix} \begin{Bmatrix} \delta\mathbf{v}_m \\ \delta\mathbf{p} \\ \delta\boldsymbol{\rho}_m \\ \delta\tilde{\boldsymbol{\rho}}_m \end{Bmatrix} + \begin{pmatrix} 0 & 0 & \mathbf{C}_{13} & \mathbf{C}_{14} \\ \mathbf{C}_{21} & 0 & \mathbf{C}_{23} & \mathbf{C}_{24} \\ \mathbf{C}_{31} & \mathbf{C}_{32} & \mathbf{C}_{33} & \mathbf{C}_{34} \\ \mathbf{C}_{41} & \mathbf{C}_{42} & \mathbf{C}_{43} & \mathbf{C}_{44} \end{pmatrix} \begin{Bmatrix} \delta\dot{\mathbf{v}}_m \\ \delta\dot{\mathbf{p}} \\ \delta\dot{\boldsymbol{\rho}}_m \\ \delta\dot{\tilde{\boldsymbol{\rho}}}_m \end{Bmatrix}$$
$$= \begin{Bmatrix} \mathbf{f}_1 \\ \mathbf{f}_2 \\ \mathbf{f}_3 \\ \mathbf{f}_4 \end{Bmatrix} - \begin{pmatrix} \mathbf{K}_{11}^0 & 0 & 0 & 0 \\ \mathbf{K}_{21}^0 & \mathbf{K}_{22}^0 & \mathbf{K}_{23}^0 & \mathbf{K}_{24}^0 \\ \mathbf{K}_{31}^0 & 0 & \mathbf{K}_{33}^0 & \mathbf{K}_{34}^0 \\ \mathbf{K}_{41}^0 & 0 & \mathbf{K}_{43}^0 & \mathbf{K}_{44}^0 \end{pmatrix} \begin{Bmatrix} \mathbf{v}_m^r \\ \mathbf{p}^r \\ \boldsymbol{\rho}_m^r \\ \tilde{\boldsymbol{\rho}}_m^r \end{Bmatrix} - \begin{pmatrix} 0 & 0 & \mathbf{C}_{13}^0 & \mathbf{C}_{14}^0 \\ \mathbf{C}_{21}^0 & 0 & \mathbf{C}_{23}^0 & \mathbf{C}_{24}^0 \\ \mathbf{C}_{31}^0 & \mathbf{C}_{32}^0 & \mathbf{C}_{33}^0 & \mathbf{C}_{34}^0 \\ \mathbf{C}_{41}^0 & \mathbf{C}_{42}^0 & \mathbf{C}_{43}^0 & \mathbf{C}_{44}^0 \end{pmatrix} \begin{Bmatrix} \dot{\mathbf{v}}_m^r \\ \dot{\mathbf{p}}^r \\ \dot{\boldsymbol{\rho}}_m^r \\ \dot{\tilde{\boldsymbol{\rho}}}_m^r \end{Bmatrix} \tag{60}$$

The matrix entries of this equation are given in Appendix C.

Eq. (60) contains an extra degree of freedom as compared to that if the standard Galerkin method is utilized to discretize all variables. This entails that the system of equations that needs to be solved is larger. However, this increase is minor, as the extra degree of freedom is only added to the nodes where the element is intersected by the interface between air and CO_2. Moreover, this increase in the system size is compensated by the advantages of the partition of unity method, which is effectively mesh-independent that allows for the utilization of relatively coarse meshes.

Eq. (60) is solved using fully implicit time integration scheme.

7 Numerical examples

Two numerical examples simulating CO_2 leakage through an abandoned wellbores are solved using the proposed PUM-SG model. The first numerical example is designed to simulate initial and boundary conditions normally existing in typical CO_2 geosequestration sites, and the second numerical example is designed to simulate an extreme boundary condition that results to phase changes and a complicated mixture of fluids through the wellbore. The computational efficiency of the model and its capability to simulate phase changes are highlighted.

7.1 CO_2 leakage: normal boundary conditions

This example simulates CO_2 leakage through an abandoned wellbore subjected to initial and boundary conditions typically existing in CO_2 geosequestration sites. Fig. 2 shows the wellbore geometry and its boundary conditions, and Table 1 shows its properties, together with the properties of the surrounding formation. The objective of this example is to examine the model computational efficiency and its mesh-independency.

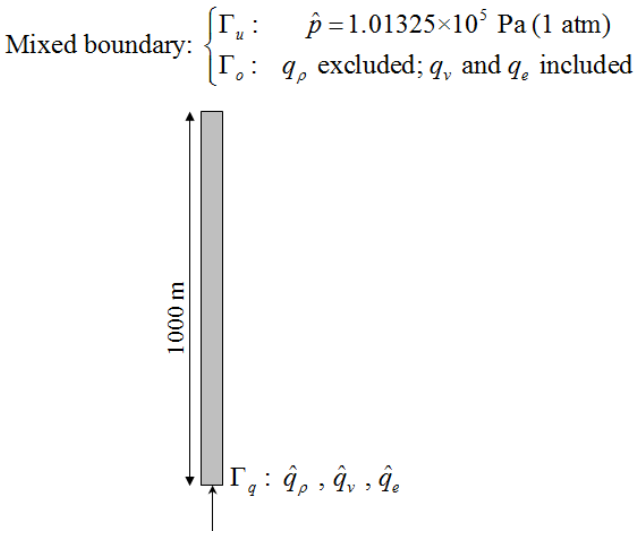

Fig. 2 Geometry and boundary conditions for the CO_2 blowout example.

Table 1 Wellbore and formation data.

Well Data	
Deviation angle [degree]	90
Well inner radius [m]	0.1
Well casing thickness [m]	0.02
Casing thermal conductivity [W m^{-1} K^{-1}]	0.6
Roughness of the wellbore [-]	5.0×10^{-6}
Formation Data	
Surface temperature [K]	275.15
Geothermal Gradient [K/m]	0.058

Initially, the wellbore is filled with air, which is under mechanical equilibrium with the atmosphere on the top, and in thermal equilibrium with the surrounding formation. The thermodynamic state of CO_2 in the reservoir is supercritical with $p = 7.5$ MPa and $\rho = 250$ kg/m^3. The CO_2 leakage rate at the bottom-hole is a function of the reservoir pressure, as

$$v_m = \frac{k_p}{\mu_{\mathrm{co}_2}}\left(p_R - p\big|_{z=z_b}\right) \tag{61}$$

where p_R is the local reservoir pressure, and z_b is the coordinate of the bottom-hole, and k_p is the effective permeability of the defective cement plug, assumed 4×10^{-13} m^2.

This problem is solved using four mesh sizes: 4, 10, 20 and 100, 1D linear finite elements.

Fig. 3 shows the computational results of the mixture density at four different points of time before the CO_2 front reaches the top of the wellbore. Apparently, the results are very close to each other, especially those of the 20 elements mesh and the 100 elements mesh. Additionally, the model is capable of capturing the sharp front between the CO_2 and air, even with relatively coarse meshes. This clearly implies that the model is computationally efficient and effectively mesh-independent.

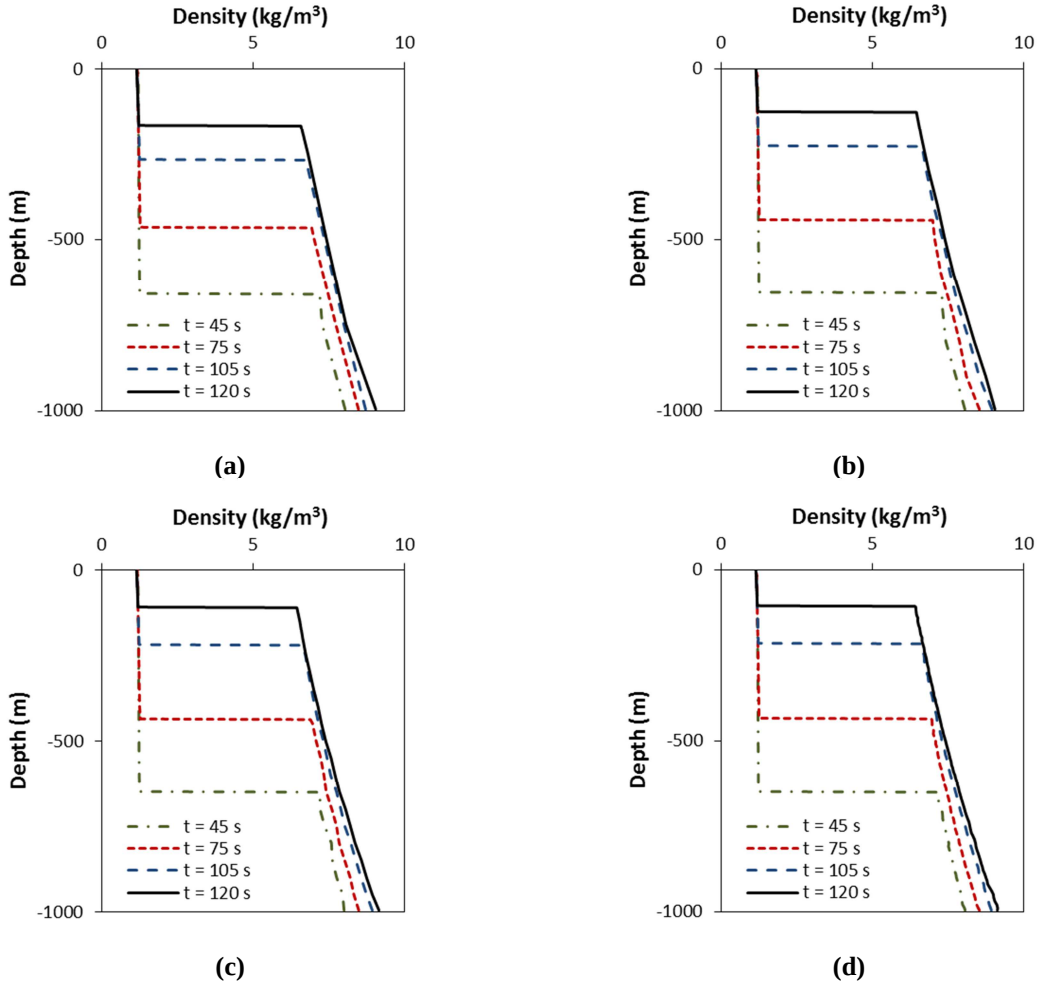

Fig. 3 Mixture density at four different points of time: (a) 4 elements, (b) 10 elements, (c) 20 elements, (d) 100 elements.

Fig. 4 shows the velocity, pressure and temperature distributions along the wellbore for the 20 elements mesh. The figure clearly shows that the velocity and pressure fields are continuous over the domain, as stated in Eq. (1), but the temperature field is discontinues due its direct relationship to the fluid density, as stated in Section 4.2. The plot of temperature shows that the temperature drops as low as 271 K (-2.15 ºC) which is 62.15 degrees less than the reservoir temperature. This drop in temperature is attributed to that, upon leaking of a supercritical CO_2, an immediate expansion of CO_2 takes place, giving rise to a sudden reduction of temperature due to the Joule–Thomson effect.

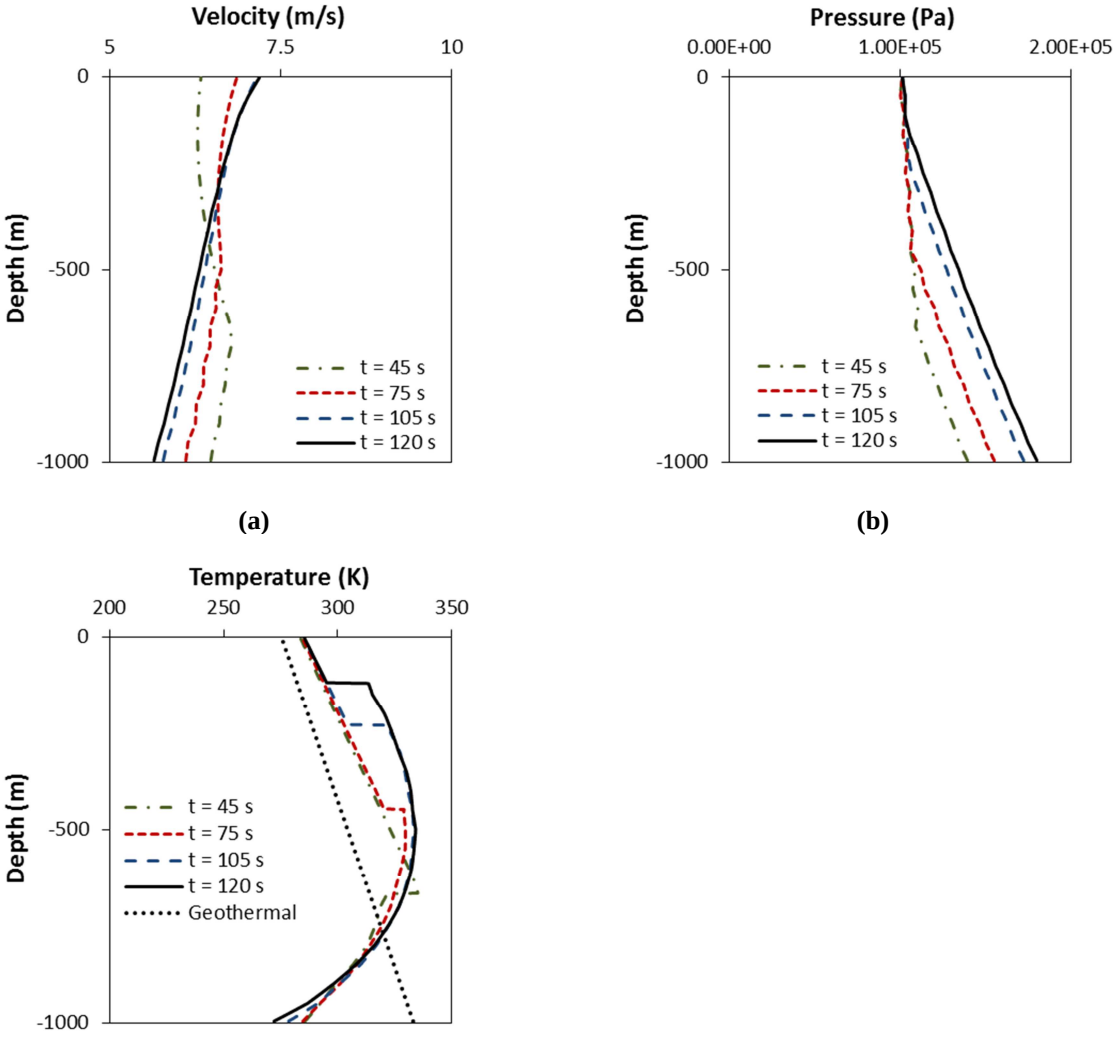

Fig. 4 Computational results using 20 elements: (a) mixture velocity, (b) pressure, (c) temperature.

7.2 CO_2 leakage: extreme boundary conditions

This example simulates CO_2 leakage through an abandoned wellbore subjected to extreme boundary conditions. Fig. 5 shows the wellbore geometry and its boundary conditions. The properties of the wellbore and the surrounding formation are as those given in Table 1. The initial conditions are similar to that of the previous numerical example. The objective of this example is to examine the model computational capability to simulate extreme boundary conditions, which lead to phase changes and complicated flow pattern along the wellbore.

The CO_2 leakage rate at the bottom-hole is assumed to have a constant velocity, but exhibiting an increasing pressure and density, as

$$\hat{v}_m = 1 \text{ m/s} \tag{62}$$

$$\hat{p} = \begin{cases} 1.114575\times10^5 + 4.44427125\times10^3 t & t < 2000 \text{ s} \\ 9\times10^6 & t \geq 2000 \text{ s} \end{cases} \quad \text{Pa} \tag{63}$$

$$\hat{\rho}_m = \begin{cases} 10 + 0.27t & t < 2000 \text{ s} \\ 550 & t \geq 2000 \text{ s} \end{cases} \quad \text{kg/m}^3 \tag{64}$$

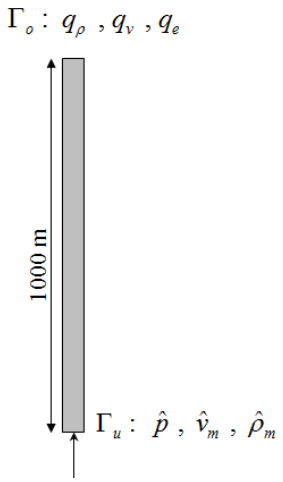

Fig. 5 Geometry and boundary conditions for the CO_2 leakage problem with extreme boundary conditions.

This problem is solved using 100, 1D linear elements.

Fig. 6 shows the CO_2 gas/liquid phase distribution along the wellbore versus time. The figure shows that, immediately, after the start of leakage, the CO_2 gas displaces the air and a gas/liquid mixture starts to form at the bottom of the wellbore. Until approximately 750 s, the wellbore is occupied by air, gas CO_2 and gas/liquid mixture CO_2. After 1500 s, a liquid CO_2 starts to form at the wellbore bottom, shortly followed by a supercritical CO_2. After approximately 2000 s, the pure gas state disappears and the wellbore becomes occupied by CO_2 liquid/gas mixture, liquid CO_2 and supercritical CO_2.

Fig. 7 shows the projection of the CO_2 states on the CO_2 phase diagram over the length of wellbore at four different times marked by dashed-lines in Fig. 6. The phase diagram is plotted using Eq. (B.1). At times t = 1000 s and t = 1500 s, the computed $p-\rho$ curve goes through liquid/gas mixture to pure gas zone. At t = 1750 s, the p-ρ curve goes through supercritical CO_2, liquid CO_2, liquid/gas mixture and pure gas zones. At t = 4500 s, the $p-\rho$ curve goes through supercritical CO_2, liquid CO_2 and liquid/gas CO_2 zones. The pure gas in this interval has already disappeared.

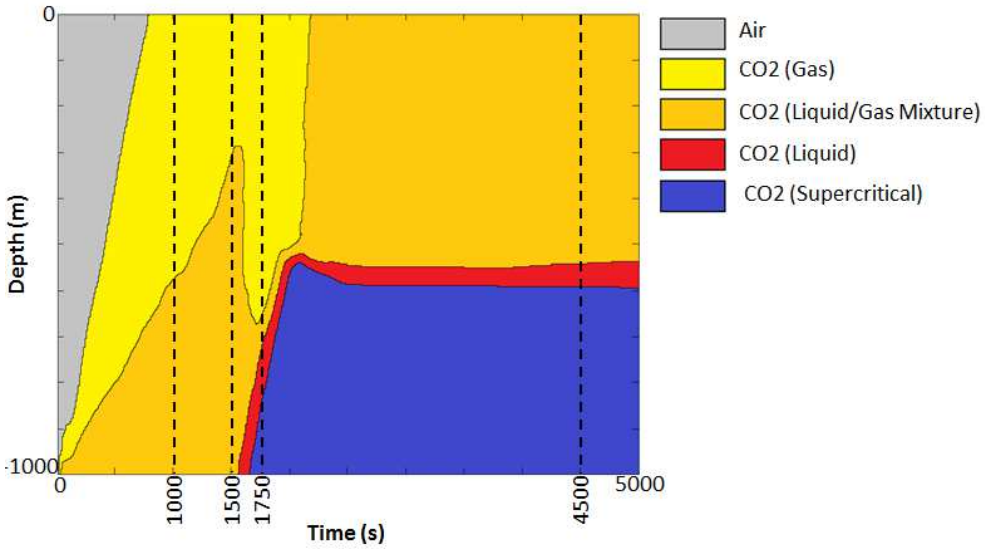

Fig. 6 Fluid and phase distribution over time.

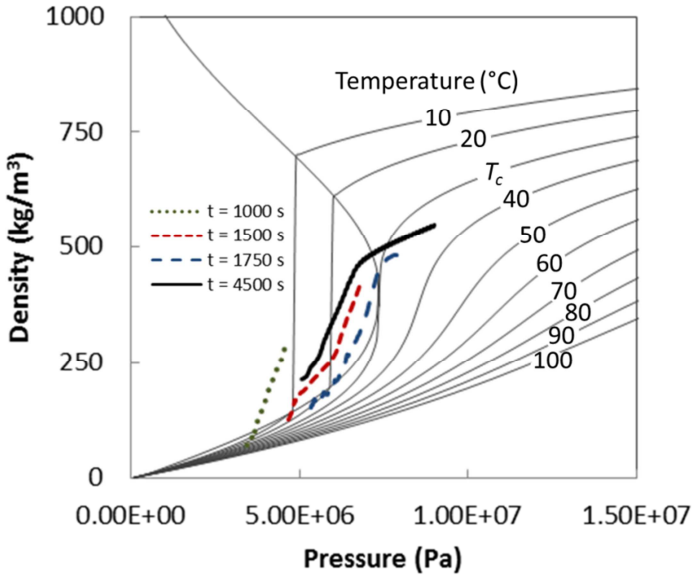

Fig. 7 Projections of the CO_2 state into the phase diagram of CO_2 over the length of wellbore.

8 Conclusions

Leakage of CO_2 to the ground surface via abandoned wellbores is hazardous and considered as one of the main concerns of applying CO_2 geosequestration technology. It is therefore vital to develop accurate computational tools capable of modelling this kind of leakage. As the problem occurs at a regional level, it is also vital that the tool be computationally efficient and mesh-independent. Solving this problem constitutes the focal point of this paper.

Developing an accurate, mesh-independent and computationally efficient transient model for such a problem is challenging due to the presence of fluid dynamics, buoyancy, phase change, compressibility, thermal interactions, wall friction and slip between phases along the wellbore. In this

paper, we show that solving this problem requires an innovative coupling between the theoretical formulation and the numerical procedure. Both, averaging techniques and tailored numerical discretization procedures are necessary. The drift-flux model is utilized to formulate the problem, and a mixed discretization scheme, integrating the standard Galerkin finite element method, the partition of unity method, and the level-set method, is utilized to solve the problem. A one dimensional compressible two-fluid domain, representing a homogeneous air gas and a mixture CO_2 with a jump at the interface between them, is modeled. All important physical phenomena and processes are considered.

The computational model is tested by solving two numerical examples with different boundary conditions. The computational results clearly exhibit the occurrence of phase change along the wellbore, the extent of which depends on the boundary conditions and the thermodynamic properties of CO_2. The paper shows that the proposed computational model is computationally efficient and effectively mesh-independent.

Acknowledgements

The authors acknowledge the financial support by Agentschap NL (Dutch Ministry of Economic Affairs) under grant number EOSLT07040.

Appendix A: Drift flux model parameters

The drift flux model parameters are defined as follows:

The wall friction coefficient can be defined as [1]:

$$f=\begin{cases}\dfrac{16}{\mathrm{Re}} & \mathrm{Re}<2400\\ \dfrac{1}{16}\left\{\log\left[\dfrac{\varepsilon}{3.7r_i}-\dfrac{5.02}{\mathrm{Re}}\log\left(\dfrac{\varepsilon}{3.7r_i}+\dfrac{13}{\mathrm{Re}}\right)\right]\right\}^{-2} & \mathrm{Re}\geq 2400\end{cases} \tag{A.1}$$

where ε is the roughness of the wellbore, and Re is the Reynolds number given by

$$\mathrm{Re}=\frac{\rho_m\left|v_m\right|(2r_i)}{\mu_m} \tag{A.2}$$

The heat exchange between the well and the surrounding formation can be described as

$$Q=2\pi r_w U\left(T-T_e\left(z\right)\right) \tag{A.3}$$

in which $T_e\left(z\right)$ is the formation temperature, and U is the overall thermal interaction coefficient of the wellbore, which can be described as [27]:

$$U=\frac{1}{R_{\mathrm{conv}}+R_{\mathrm{cond}}} \tag{A.4}$$

where R_{conv} and R_{cond} are the thermal resistances of the fluid and casing material, respectively, described as

$$R_{\mathrm{conv}}=r_o\big/\left(r_w\bar{h}\right) \tag{A.5}$$

$$R_{\mathrm{cond}}=r_o\ln\left(r_o/r_w\right)\big/\lambda_p \tag{A.6}$$

in which r_o is the outer radius of the wellbore, λ_p is the thermal conductivity of the casing material, and $\bar{h}$ is the convective heat transfer coefficient, described as

$$\bar{h}=\mathrm{Nu}\,\lambda_m\big/(2r_i) \tag{A.7}$$

where Nu is the Nusselt number, defined as

$$\mathrm{Nu}=\begin{cases}0.664\,\mathrm{Re}^{1/2}\,\mathrm{Pr}^{1/3} & \mathrm{Re}\leq 2000\\ 0.023\,\mathrm{Re}^{0.8}\,\mathrm{Pr}^{0.4} & \mathrm{Re}>2000\end{cases} \tag{A.8}$$

in which Pr is the Prandtl number given by

$$\mathrm{Pr}=\frac{\nu}{\alpha}=\frac{\mu_m/\rho_m}{\lambda_m/\left(\rho_m c_{pm}\right)}=\frac{\mu_m c_{pm}}{\lambda_m} \tag{A.9}$$

where c_{pm} and λ_m are the specific isobaric heat capacity and thermal conductivity of the mixture, respectively.

The slip parameter γ is defined as [28]

$$\gamma\left(v_m, p, \rho_m\right)=\frac{f_G}{1-f_G}\frac{\rho_G\rho_L\rho_m}{\rho_m^{*2}}\left[\left(C_0-1\right)v_m+v_d\right]^2 \tag{A.10}$$

in which f_G is the gas volume fraction, ρ_G is the gas density, ρ_L is the liquid density, v_d is the drift velocity, and

$$\rho_m^*=f_G C_0\rho_G+\left(1-f_G C_0\right)\rho_L \tag{A.11}$$

The drift velocity describes the variance in velocities between phases of a mixture. It can be described as [17]:

$$v_d\left(v_m, p, \rho_m\right)=\frac{\left(1-C_0 f_G\right)v_c K\left(f_G, K_u, C_0\right)m(\theta)}{C_0 f_G\sqrt{\rho_G/\rho_L}+1-C_0 f_G} \tag{A.12}$$

where:

- $m(\theta)$ is an inclination adjusting function, described as

$$m(\theta)=m_0\left(\cos\theta\right)^{n_1}\left(1+\sin\theta\right)^{n_2} \tag{A.13}$$

in which m_0, n_1, and n_2 are fitting parameters.

- K_u is the Kutateladze number, described as

$$K_u=\left[\frac{C_{ku}}{\sqrt{N_B}}\left(\sqrt{1+\frac{N_B}{C_{ku}^2 C_w}}-1\right)\right]^{\frac{1}{2}} \tag{A.14}$$

in which $C_w=0.008$ and $C_{ku}=142$ [10], and N_B is the Bond number, defined as

$$N_B=4r_i^2\left[\frac{g\left(\rho_L-\rho_G\right)}{\sigma_{GL}}\right] \tag{A.15}$$

where σ_{GL} is the gas-liquid surface tension.

- v_c is the characteristic velocity, given by

$$v_c = \left[\frac{g\sigma_{GL}\left(\rho_L - \rho_G\right)}{\rho_L^2}\right]^{\frac{1}{4}} \tag{A.16}$$

- K is a smooth transition function, introduced to make a smooth transition of the drift velocity between the bubble rise and the film flooding flow regimes, described as [10]:

$$K = \begin{cases} 1.53 & f_G \le a_1 \\ 1.53 + \dfrac{C_0 K_u - 1.53}{2}\left[1 - \cos\left(\pi \dfrac{f_G - a_1}{a_2 - a_1}\right)\right] & a_1 \le f_G \le a_2 \\ C_0 K_u & f_G \ge a_2 \end{cases} \tag{A.17}$$

in which a_1 and a_2 are two transitional gas volume fractions corresponding to the bubble rise and the film flooding flow regimes, respectively.

- C_0 is a profile parameter, calculated as [17]:

$$C_0 = \frac{C_{\max}}{1 + \left(C_{\max} - 1\right)\eta^2} \tag{A.18}$$

in which $C_{\max}$ is the profile parameter for low gas fraction and η is a parameter reflecting the effect of the flow status on the profile parameter, given by:

$$\eta = \frac{\beta - B}{1 - B} \tag{A.19}$$

where B is the threshold parameter above which C_0 starts to drop below $C_{\max}$, described as [10]:

$$B = \frac{2}{C_{\max}} - 1.0667 \tag{A.20}$$

and β is calculated as

$$\beta = \max\left(f_G, F_V \frac{f_G \left|v_m\right|}{v_{sgf}}\right) \quad , \quad 0 \le \beta \le 1 \tag{A.21}$$

in which F_V is a multiplier to adjust the sensitivity of the profile flattening to the gas velocity, and v_{sgf} is a gas superficial velocity at which flooding occurs. F_V is equal to 1, according to Shi *et al.* [17], and v_{sgf} is calculated as:

$$v_{sgf} = K_u \left(\frac{\rho_L}{\rho_G}\right)^{\frac{1}{2}} v_c \tag{A.22}$$

Since there is no experimental data to determine the fitting parameters $C_{\max}$, m_0, n_1, n_2, a_1 and a_2, the available values for water-gas mixture is used instead, that read: $C_{\max}=1$, $m_0=1.85$ $n_1=0.21$, $n_2=0.95$, $a_1=0.06$, and $a_2=0.21$ [17].

Appendix B: Constitutive equations

B.1 CO_2 constitutive equations

Sequestrated CO_2 in a geological formation most likely exists in a supercritical state. When the CO_2 plume reaches an abandoned wellbore and leaks into it, the CO_2 phase can change from its initial supercritical state to liquid, liquid/gas mixture or gas, depending on the pressure and temperature conditions at any certain level in the wellbore. Fig. B.1 shows the phase diagram of CO_2. According to this diagram, if the temperature and pressure drop below the critical values, $T_C^{co_2} = 304.1\,\text{K}$ and $p_C^{co_2} = 7.38\,\text{MPa}\ (73.8\ \text{bar})$, the CO_2 phase changes to liquid, gas or a liquid/gas mixture. The liquid/gas mixture is formed when the pressure equals to the "saturated vapor pressure"; i.e. the pressure at which the gas (vapor) phase and the liquid phase are in thermodynamic equilibrium (along the solid line between the liquid and gas phases in the phase diagram).

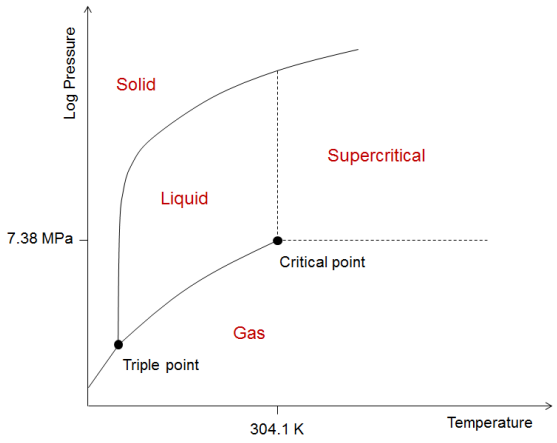

Fig. B.1 CO_2 pressure-temperature phase diagram.

Thus, the CO_2 constitutive properties must cover all phases that might be formed along the wellbore, including supercritical, liquid, gas and liquid/gas mixture (saturated vapor region).

Equation of state

We use the Redlich and Kwong [29] equation of state, given as

$$p = \frac{RT}{V - b_{co_2}} - \frac{a_{co_2}}{T^{0.5} V \left(V + b_{co_2}\right)} \tag{B.1}$$

where V is the molar volume of the CO_2 phase, R is the universal gas constant ($= 8.314462\ \text{J/(mol K)}$), and a_{co_2} and b_{co_2} are the intermolecular attraction and repulsion, respectively. Spycher *et al.* [30] utilized experimental data to evaluate these parameters, giving

$$\begin{aligned} a_{co_2} &= 7.54 - 4.13\times10^{-3} T \quad \text{Pa m}^6\ \text{K}^{0.5}\ \text{mol}^{-2} \\ b_{co_2} &= 27.8\times10^{-6} \quad \text{m}^3/\text{mol} \end{aligned} \tag{B.2}$$

The molar volume - density relationship is defined as

$$\rho = \frac{M_{co_2}}{V} \tag{B.3}$$

where M_{co_2} is the molar mass of CO_2 ($= 44 \times 10^{-3}$ kg/mol).

Substituting Eq. (B.3) into Equation (B.1), after rearrangement, yields

$$\left(\frac{a_{co_2} b_{co_2}}{pT^{0.5}}\right)\rho^3 + M_{co_2}\left(\frac{RTb_{co_2}}{p} - \frac{a_{co_2}}{pT^{0.5}} + b_{co_2}^{\ 2}\right)\rho^2 + M_{co_2}^{\ 2}\left(\frac{RT}{p}\right)\rho - M_{co_2}^{\ 3} = 0 \tag{B.4}$$

Using this equation, any of the three thermodynamic variables of CO_2; temperature, density and pressure; can be calculated as a function of the other two. For the liquid/vapor mixture, the averaged mixture density is used in this equation. Fig. B.2 shows three isothermal curves for CO_2. The figure clearly shows the supercritical behavior of CO_2 for temperatures: T = 50°C and T = 70°C, where the gas and the fluid are combined to form a single fluid. For T = 30°C, there is a sharp transition between the vapor phase and the saturated liquid phase.

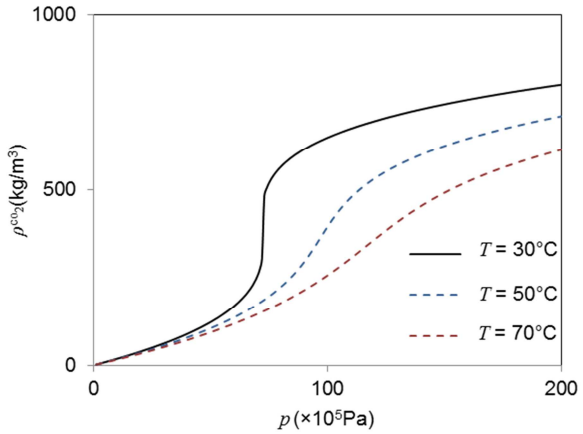

Fig. B.2 Isothermal curves of CO_2 in density-pressure phase diagram.

Specific enthalpy

The CO_2 specific enthalpy presented by Span and Wagner [31] is utilized. It reads

$$h = RT\left(1 + \tau\left(\frac{\partial f^0}{\partial \tau} + \frac{\partial f^r}{\partial \tau}\right) + \delta\frac{\partial f^r}{\partial \delta}\right) \tag{B.5}$$

with f^0 representing the Helmholtz energy of an ideal gas, and f^r representing the residual part of the Helmholtz energy. They are functions of temperature and density, as

$$f^0(\delta,\tau) = \ln(\delta) + a_1^\circ + a_2^\circ\tau + a_3^\circ \ln(\tau) + \sum_{i=4}^{8} a_i^\circ \ln\left[1 - \exp\left(-\tau\theta_i^\circ\right)\right] \tag{B.6}$$

and

$$f^r(\delta,\tau)=\sum_{i=1}^{7} n_i \delta^{d_i}\tau^{t_i} + \sum_{i=8}^{34} n_i \delta^{d_i}\tau^{t_i} e^{-\delta^{c_i}} + \sum_{i=35}^{39} n_i \delta^{d_i}\tau^{t_i} e^{-\alpha_i(\delta-\varepsilon_i)^2-\beta_i(\tau-\gamma_i)^2} + \sum_{i=40}^{42} n_i \Delta^{b_i}\delta e^{-C_i(\delta-1)^2-D_i(\tau-1)^2} \quad \text{(B.7)}$$

with

$$\Delta=\left\{(1-\tau)+A_i\left[(\delta-1)^2\right]^{1/(2\beta_i)}\right\}^2 + B_i\left[(\delta-1)^2\right]^{a_i} \quad \text{(B.8)}$$

where $\tau = T_C^{co_2} / T$ and $\delta = \rho / \rho_C^{co_2}$ are the inverse reduced temperature and reduced density, respectively; and $\rho_C^{co_2}$ is the CO_2 density at the critical condition. The reader is referred to Span and Wagner [31] to obtain the values of the coefficients a_i°, θ_i°, n_i, d_i, t_i, c_i, α_i, ε_i, β_i, γ_i, C_i, D_i, A_i, B_i and a_i.

Fig. B.3 shows the CO_2 specific enthalpy versus pressure for different temperatures. As for the density-pressure phase diagram, it shows the supercritical behavior of pure CO_2 at T = 45°C and T = 60°C, while for T = 30°C, there is a clear distinction between the gas phase and the saturated liquid phase.

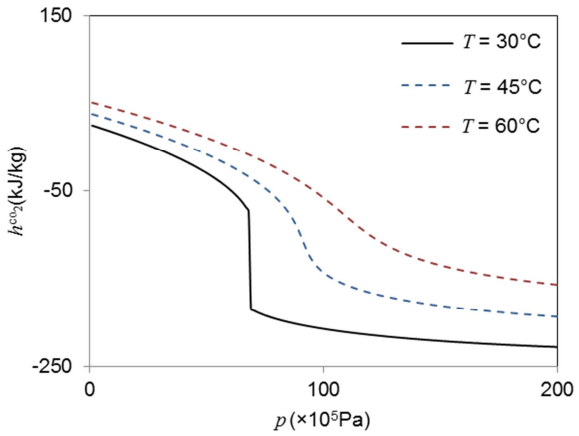

Fig. B.3 CO_2 specific enthalpy versus pressure for different temperatures

Viscosity

The CO_2 viscosity can be determined following Fenghour *et al.* [32], as:

$$\mu = 1.00697\sqrt{T} \Big/ \Big[0.235156 - 0.491266 \ln \tau^* + 5.211155 \times 10^{-2} \left(\ln \tau^* \right)^2 + 5.347906 \times 10^{-2} \left(\ln \tau^* \right)^3 - 1.537102 \times 10^{-2} \left(\ln \tau^* \right)^4 \Big] + 0.4071119 \times 10^{-2} \rho + 0.7198037 \times 10^{-4} \rho^2 + \frac{0.2411697 \times 10^{-16} \rho^6}{\left(\tau^* \right)^3} + 0.2971072 \times 10^{-22} \rho^8 - 0.1627888 \times 10^{-22} \frac{\rho^8}{\tau^*} \quad \text{(B.9)}$$

in which $\tau^* = T / 251.196$ is a reduced temperature, where T is in Kelvin; ρ is the density of CO_2 in $\mathrm{kg/m^3}$; and μ is in $\mu\,\mathrm{Pa.s}$.

Fig. B.4 depicts CO_2 viscosity versus pressure for three different temperatures. A similar trend in phase change as that for the CO_2 density, Fig. B.2, can be observed.

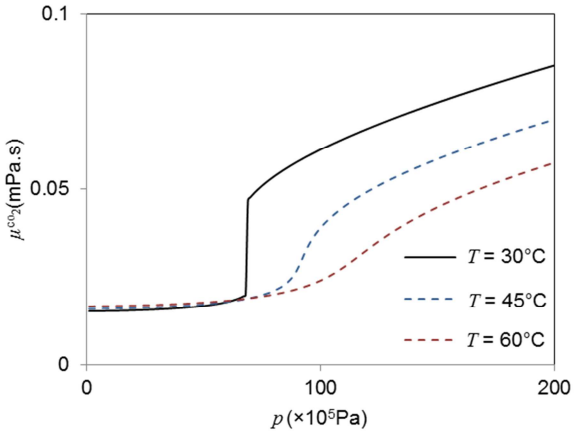

Fig. B.4 CO_2 viscosity versus pressure for three different temperatures.

B.2 Air constitutive equations

The air is assumed to be always in a gaseous phase in the wellbore, and hence the ideal gas law is utilized to establish its constitutive equations.

Equation of state

Based on the ideal gas theory, the relationship between density, pressure and temperature of air can be described as

$$p = \frac{\rho R T}{M_{air}} \quad \text{(B.10)}$$

where M_{air} is the molar mass of air ($= 28.97 \times 10^{-3}$ kg/mol).

Specific enthalpy

The enthalpy of air as an ideal gas is given by

$$h = c_p^{\text{air}} T \tag{B.11}$$

in which c_p^{air} is the specific isobaric heat capacity ($= 1006$ J/(kg K)).

Viscosity

The viscosity of air is given by Sutherland's relation [33], as

$$\mu = 1.46\left(\frac{T^{3/2}}{T+111}\right) \tag{B.12}$$

where T is in Kelvin and μ is in μPa.s.

Appendix C. Components of the finite element matrices

$$\mathbf{K}_{11} = -\int_{\Omega} \mathbf{B}^T \rho_m^r \mathbf{N} d\Omega + \int_{\Gamma_d} \mathbf{N}^T \rho_{\mathrm{co}_2}^r \mathbf{N} \cdot n \, d\Gamma - \int_{\Gamma_d} \mathbf{N}^T \rho_{\mathrm{air}}^r \mathbf{N} \cdot n \, d\Gamma + \int_{\Gamma_o} \mathbf{N}^T \rho_m^r \mathbf{N} \cdot n \, d\Gamma \tag{C.1}$$

$$\mathbf{K}_{13} = -\int_{\Omega} \mathbf{B}^T v_m^r \mathbf{N} d\Omega + \int_{\Gamma_o} \mathbf{N}^T v_m^r \mathbf{N} \cdot n \, d\Gamma \tag{C.2}$$

$$\mathbf{K}_{14} = -\int_{\Omega} \mathbf{B}^T v_m^r \mathbf{N}^{eh} d\Omega + \int_{\Gamma_d} \mathbf{N}^T v_m^r \mathbf{N}^{eh+} \cdot n \, d\Gamma - \int_{\Gamma_d} \mathbf{N}^T v_m^r \mathbf{N}^{eh-} \cdot n \, d\Gamma + \int_{\Gamma_o} \mathbf{N}^T v_m^r \mathbf{N}^{eh} \cdot n \, d\Gamma \tag{C.3}$$

$$\mathbf{C}_{13} = \int_{\Omega} \mathbf{N}^T \mathbf{N} d\Omega \tag{C.4}$$

$$\mathbf{C}_{14} = \int_{\Omega} \mathbf{N}^T \mathbf{N}^{eh} d\Omega \tag{C.5}$$

$$\mathbf{K}_{11}^0 = -\int_{\Omega} \mathbf{B}^T \rho_m^r \mathbf{N} d\Omega + \int_{\Gamma_d} \mathbf{N}^T \rho_{\mathrm{co}_2}^r \mathbf{N} \cdot n \, d\Gamma - \int_{\Gamma_d} \mathbf{N}^T \rho_{\mathrm{air}}^r \mathbf{N} \cdot n \, d\Gamma + \int_{\Gamma_o} \mathbf{N}^T \rho_m^r \mathbf{N} \cdot n \, d\Gamma \tag{C.6}$$

$$\mathbf{C}_{13}^0 = \int_{\Omega} \mathbf{N}^T \mathbf{N} d\Omega \tag{C.7}$$

$$\mathbf{C}_{14}^0 = \int_{\Omega} \mathbf{N}^T \mathbf{N}^{eh} d\Omega \tag{C.8}$$

$$\mathbf{f}_1 = -\int_{\Gamma_q} \mathbf{N}^T \hat{q}_\rho d\Gamma \tag{C.9}$$

$$\begin{aligned}
\mathbf{K}_{21} &= \int_{\Omega} \mathbf{N}^T \dot{\rho}_m^r \mathbf{N} d\Omega - \int_{\Omega} 2\mathbf{B}^T \rho_m^r v_m^r \mathbf{N} d\Omega - \int_{\Omega} \mathbf{B}^T \frac{\partial \gamma^r}{\partial v_m} \mathbf{N} d\Omega \\
&+ \int_{\Omega} \mathbf{N}^T \frac{f^r}{2r_i} \rho_m^r \mathrm{sign}\left(v_m^r\right) v_m^r \mathbf{N} d\Omega \\
&+ \int_{\Omega} \mathbf{N}^T \frac{1}{4r_i} \frac{\rho_m^r \mathrm{sign}\left(v_m^r\right)(2r_i)}{\mu_m^r} \frac{\partial f^r}{\partial \mathrm{Re}} \rho_m^r \mathrm{sign}\left(v_m^r\right)\left(v_m^r\right)^2 \mathbf{N} d\Omega + \int_{\Gamma_d} 2\mathbf{N}^T \rho_{\mathrm{co}_2}^r v_m^r \mathbf{N} \cdot n \, d\Gamma \\
&- \int_{\Gamma_d} 2\mathbf{N}^T \rho_{\mathrm{air}}^r v_m^r \mathbf{N} \cdot n \, d\Gamma + \int_{\Gamma_o} 2\mathbf{N}^T \rho_m^r v_m^r \mathbf{N} \cdot n \, d\Gamma + \int_{\Gamma_o} \mathbf{N}^T \frac{\partial \gamma^r}{\partial v_m} \mathbf{N} \cdot n \, d\Gamma
\end{aligned} \tag{C.10}$$

$$\mathbf{K}_{22} = \int_{\Omega} \mathbf{N}^T \mathbf{B} d\Omega \tag{C.11}$$

$$\mathbf{K}_{23} = \int_{\Omega} \mathbf{N}^T \dot{v}_m^r \mathbf{N} d\Omega - \int_{\Omega} \mathbf{B}^T \left(v_m^r\right)^2 \mathbf{N} d\Omega - \int_{\Omega} \mathbf{B}^T \frac{\partial \gamma^r}{\partial \rho_m} \mathbf{N} d\Omega$$
$$+ \int_{\Omega} \mathbf{N}^T \frac{f^r}{4r_i} \operatorname{sign}\left(v_m^r\right)\left(v_m^r\right)^2 \mathbf{N} d\Omega + \int_{\Omega} \mathbf{N}^T \mathbf{N} g \sin\theta d\Omega$$
$$+ \int_{\Omega} \mathbf{N}^T \frac{1}{4r_i} \left(\frac{\left|v_m^r\right|(2r_i)}{\mu_m^r} - \frac{\rho_m^r \left|v_m^r\right|(2r_i)}{\left(\mu_m^r\right)^2} \frac{\partial \mu_m^r}{\partial \rho_m} \right) \frac{\partial f^r}{\partial \operatorname{Re}} \rho_m^r \operatorname{sign}\left(v_m^r\right)\left(v_m^r\right)^2 \mathbf{N} d\Omega \quad \text{(C.12)}$$
$$+ \int_{\Gamma_o} \mathbf{N}^T \left(v_m^r\right)^2 \mathbf{N} \cdot n \, d\Gamma + \int_{\Gamma_o} \mathbf{N}^T \frac{\partial \gamma^r}{\partial \rho_m} \mathbf{N} \cdot n \, d\Gamma$$

$$\mathbf{K}_{24} = \int_{\Omega} \mathbf{N}^T \dot{v}_m^r \mathbf{N}^{eh} d\Omega - \int_{\Omega} \mathbf{B}^T \left(v_m^r\right)^2 \mathbf{N}^{eh} d\Omega - \int_{\Omega} \mathbf{B}^T \frac{\partial \gamma^r}{\partial \rho_m} \mathbf{N}^{eh} d\Omega$$
$$+ \int_{\Omega} \mathbf{N}^T \frac{f^r}{4r_i} \operatorname{sign}\left(v_m^r\right)\left(v_m^r\right)^2 \mathbf{N}^{eh} d\Omega + \int_{\Omega} \mathbf{N}^T \mathbf{N}^{eh} g \sin\theta d\Omega$$
$$+ \int_{\Omega} \mathbf{N}^T \frac{1}{4r_i} \left(\frac{\left|v_m^r\right|(2r_i)}{\mu_m^r} - \frac{\rho_m^r \left|v_m^r\right|(2r_i)}{\left(\mu_m^r\right)^2} \frac{\partial \mu_m^r}{\partial \rho_m} \right) \frac{\partial f^r}{\partial \operatorname{Re}} \rho_m^r \operatorname{sign}\left(v_m^r\right)\left(v_m^r\right)^2 \mathbf{N}^{eh} d\Omega \quad \text{(C.13)}$$
$$+ \int_{\Gamma_d} \mathbf{N}^T \left(v_m^r\right)^2 \mathbf{N}^{eh+} \cdot n \, d\Gamma - \int_{\Gamma_d} \mathbf{N}^T \left(v_m^r\right)^2 \mathbf{N}^{eh-} \cdot n \, d\Gamma + \int_{\Gamma_o} \mathbf{N}^T \left(v_m^r\right)^2 \mathbf{N}^{eh} \cdot n \, d\Gamma$$
$$+ \int_{\Gamma_o} \mathbf{N}^T \frac{\partial \gamma^r}{\partial \rho_m} \mathbf{N}^{eh} \cdot n \, d\Gamma$$

$$\mathbf{C}_{21} = \int_{\Omega} \mathbf{N}^T \rho_m^r \mathbf{N} d\Omega \quad \text{(C.14)}$$

$$\mathbf{C}_{23} = \int_{\Omega} \mathbf{N}^T v_m^r \mathbf{N} d\Omega \quad \text{(C.15)}$$

$$\mathbf{C}_{24} = \int_{\Omega} \mathbf{N}^T v_m^r \mathbf{N}^{eh} d\Omega \quad \text{(C.16)}$$

$$\mathbf{K}_{21}^0 = -\int_{\Omega} \mathbf{B}^T \rho_m^r v_m^r \mathbf{N} d\Omega + \int_{\Omega} \mathbf{N}^T \frac{f^r}{4r_i} \rho_m^r \operatorname{sign}\left(v_m^r\right) v_m^r \mathbf{N} d\Omega \quad \text{(C.17)}$$

$$\mathbf{K}_{22}^0 = \int_{\Omega} \mathbf{N}^T \mathbf{B} \, d\Omega \quad \text{(C.18)}$$

$$\mathbf{K}_{23}^0 = \int_{\Omega} \mathbf{N}^T \mathbf{N} g \sin\theta d\Omega \quad \text{(C.19)}$$

$$\mathbf{K}_{24}^0 = \int_{\Omega} \mathbf{N}^T \mathbf{N}^{eh} g \sin\theta d\Omega \quad \text{(C.20)}$$

$$\mathbf{C}_{21}^0 = \int_{\Omega} \mathbf{N}^T \rho_m^r \mathbf{N} d\Omega \quad \text{(C.21)}$$

$$\mathbf{C}_{23}^0 = \int_{\Omega} \mathbf{N}^T v_m^r \mathbf{N} d\Omega \quad \text{(C.22)}$$

$$\mathbf{C}_{24}^{0} = \int_{\Omega} \mathbf{N}^{T} v_{m}^{r} \mathbf{N}^{eh} d\Omega \tag{C.23}$$

$$\begin{aligned}\mathbf{f}_{2} = &\int_{\Omega} \mathbf{B}^{T} \gamma^{r} d\Omega - \int_{\Gamma_{d}} \mathbf{N}^{T} \rho_{\mathrm{co}_2}^{r} \left(v_{m}^{r}\right)^{2} \cdot n \, d\Gamma + \int_{\Gamma_{d}} \mathbf{N}^{T} \rho_{\mathrm{air}}^{r} \left(v_{m}^{r}\right)^{2} \cdot n \, d\Gamma \\ &- \int_{\Gamma_{o}} \mathbf{N}^{T} \rho_{m}^{r} \left(v_{m}^{r}\right)^{2} \cdot n \, d\Gamma - \int_{\Gamma_{o}} \mathbf{N}^{T} \gamma^{r} \cdot n \, d\Gamma - \int_{\Gamma_{q}} \mathbf{N}^{T} \hat{q}_{v} d\Gamma\end{aligned} \tag{C.24}$$

$$\begin{aligned}\mathbf{K}_{31} = &\int_{\Omega} \mathbf{N}^{T} v_{m}^{r} \dot{\rho}_{m}^{r} \mathbf{N} d\Omega + \int_{\Omega} \mathbf{N}^{T} \rho_{m}^{r} \dot{v}_{m}^{r} \mathbf{N} d\Omega - \int_{\Omega} \mathbf{B}^{T} \rho_{m}^{r} \left(v_{m}^{r}\right)^{2} \mathbf{N} d\Omega \\ &- \int_{\Omega} \mathbf{B}^{T} \rho_{m}^{r} \left(h_{m}^{r} + \frac{1}{2}\left(v_{m}^{r}\right)^{2}\right) \mathbf{N} d\Omega - \int_{\Omega} \mathbf{N}^{T} \rho_{m}^{r} \mathbf{N} g \sin\theta d\Omega \\ &+ \int_{\Gamma_{d}} \mathbf{N}^{T} \rho_{\mathrm{co}_2}^{r} \left(h_{\mathrm{co}_2}^{r} + \frac{1}{2}\left(v_{m}^{r}\right)^{2}\right) \mathbf{N} \cdot n \, d\Gamma + \int_{\Gamma_{d}} \mathbf{N}^{T} \rho_{\mathrm{co}_2}^{r} \left(v_{m}^{r}\right)^{2} \mathbf{N} \cdot n \, d\Gamma \\ &- \int_{\Gamma_{d}} \mathbf{N}^{T} \rho_{\mathrm{air}}^{r} \left(h_{\mathrm{air}}^{r} + \frac{1}{2}\left(v_{m}^{r}\right)^{2}\right) \mathbf{N} \cdot n \, d\Gamma - \int_{\Gamma_{d}} \mathbf{N}^{T} \rho_{\mathrm{air}}^{r} \left(v_{m}^{r}\right)^{2} \mathbf{N} \cdot n \, d\Gamma \\ &+ \int_{\Gamma_{o}} \mathbf{N}^{T} \rho_{m}^{r} \left(h_{m}^{r} + \frac{1}{2}\left(v_{m}^{r}\right)^{2}\right) \mathbf{N} \cdot n \, d\Gamma + \int_{\Gamma_{o}} \mathbf{N}^{T} \rho_{m}^{r} \left(v_{m}^{r}\right)^{2} \mathbf{N} \cdot n \, d\Gamma\end{aligned} \tag{C.25}$$

$$\begin{aligned}\mathbf{K}_{33} = &\int_{\Omega} \mathbf{N}^{T} \frac{\partial h_{m}^{r}}{\partial \rho_{m}} \dot{\rho}_{m}^{r} \mathbf{N} d\Omega + \int_{\Omega} \mathbf{N}^{T} \frac{\partial^{2} h_{m}^{r}}{\partial \rho_{m}^{2}} \dot{\rho}_{m}^{r} \rho_{m}^{r} \mathbf{N} d\Omega - \int_{\Omega} \mathbf{N}^{T} v_{m}^{r} \mathbf{N} g \sin\theta d\Omega \\ &+ \int_{\Omega} \mathbf{N}^{T} \frac{\partial h_{m}^{r}}{\partial \rho_{m}} \dot{\rho}_{m}^{r} \mathbf{N} d\Omega + \int_{\Omega} \mathbf{N}^{T} v_{m}^{r} \dot{v}_{m}^{r} \mathbf{N} d\Omega - \int_{\Omega} \mathbf{B}^{T} \left(h_{m}^{r} + \frac{1}{2}\left(v_{m}^{r}\right)^{2}\right) v_{m}^{r} \mathbf{N} d\Omega \\ &- \int_{\Omega} \mathbf{B}^{T} \rho_{m}^{r} \frac{\partial h_{m}^{r}}{\partial \rho_{m}} v_{m}^{r} \mathbf{N} d\Omega + \int_{\Omega} \mathbf{N}^{T} \frac{1}{\pi r_{i}^{2}} \frac{dQ^{r}}{dT} \frac{\partial T^{r}}{\partial \rho_{m}} \mathbf{N} d\Omega \\ &+ \int_{\Gamma_{d}} \mathbf{N}^{T} v_{m}^{r} \left(h_{\mathrm{co}_2}^{r} + \frac{1}{2}\left(v_{m}^{r}\right)^{2}\right) \mathbf{N} \cdot n \, d\Gamma - \int_{\Gamma_{d}} \mathbf{N}^{T} v_{m}^{r} \left(h_{\mathrm{air}}^{r} + \frac{1}{2}\left(v_{m}^{r}\right)^{2}\right) \mathbf{N} \cdot n \, d\Gamma \\ &+ \int_{\Gamma_{d}} \mathbf{N}^{T} \rho_{\mathrm{co}_2}^{r} v_{m}^{r} \frac{\partial h_{\mathrm{co}_2}^{r}}{\partial \rho_{m}} \mathbf{N} \cdot n \, d\Gamma - \int_{\Gamma_{d}} \mathbf{N}^{T} \rho_{\mathrm{air}}^{r} v_{m}^{r} \frac{\partial h_{\mathrm{air}}^{r}}{\partial \rho_{m}} \mathbf{N} \cdot n \, d\Gamma \\ &+ \int_{\Gamma_{o}} \mathbf{N}^{T} v_{m}^{r} \left(h_{m}^{r} + \frac{1}{2}\left(v_{m}^{r}\right)^{2}\right) \mathbf{N} \cdot n \, d\Gamma + \int_{\Gamma_{o}} \mathbf{N}^{T} \rho_{m}^{r} v_{m}^{r} \frac{\partial h_{m}^{r}}{\partial \rho_{m}} \mathbf{N} \cdot n \, d\Gamma\end{aligned} \tag{C.26}$$

$$\begin{aligned}\mathbf{K}_{34} = &\int_{\Omega} \mathbf{N}^{T} \frac{\partial h_{m}^{r}}{\partial \rho_{m}} \dot{\rho}_{m}^{r} \mathbf{N}^{eh} d\Omega + \int_{\Omega} \mathbf{N}^{T} \frac{\partial^{2} h_{m}^{r}}{\partial \rho_{m}^{2}} \dot{\rho}_{m}^{r} \rho_{m}^{r} \mathbf{N}^{eh} d\Omega - \int_{\Omega} \mathbf{N}^{T} v_{m}^{r} \mathbf{N}^{eh} g \sin\theta d\Omega \\ &+ \int_{\Omega} \mathbf{N}^{T} \frac{\partial h_{m}^{r}}{\partial \rho_{m}} \dot{\rho}_{m}^{r} \mathbf{N}^{eh} d\Omega + \int_{\Omega} \mathbf{N}^{T} v_{m}^{r} \dot{v}_{m}^{r} \mathbf{N}^{eh} d\Omega + \int_{\Omega} \mathbf{N}^{T} \frac{1}{\pi r_{i}^{2}} \frac{dQ^{r}}{dT} \frac{\partial T^{r}}{\partial \rho_{m}} \mathbf{N}^{eh} d\Omega \\ &- \int_{\Omega} \mathbf{B}^{T} \left(h_{m}^{r} + \frac{1}{2}\left(v_{m}^{r}\right)^{2}\right) v_{m}^{r} \mathbf{N}^{eh} d\Omega - \int_{\Omega} \mathbf{B}^{T} \rho_{m}^{r} \frac{\partial h_{m}^{r}}{\partial \rho_{m}} v_{m}^{r} \mathbf{N}^{eh} d\Omega \\ &+ \int_{\Gamma_{d}} \mathbf{N}^{T} v_{m}^{r} \left(h_{\mathrm{co}_2}^{r} + \frac{1}{2}\left(v_{m}^{r}\right)^{2}\right) \mathbf{N}^{eh+} \cdot n \, d\Gamma - \int_{\Gamma_{d}} \mathbf{N}^{T} v_{\mathrm{m}}^{r} \left(h_{\mathrm{air}}^{r} + \frac{1}{2}\left(v_{\mathrm{m}}^{r}\right)^{2}\right) \mathbf{N}^{eh-} \cdot n \, d\Gamma \\ &+ \int_{\Gamma_{d}} \mathbf{N}^{T} \rho_{\mathrm{co}_2}^{r} v_{m}^{r} \frac{\partial h_{\mathrm{co}_2}^{r}}{\partial \rho_{m}} \mathbf{N}^{eh+} \cdot n \, d\Gamma - \int_{\Gamma_{d}} \mathbf{N}^{T} \rho_{\mathrm{air}}^{r} v_{\mathrm{m}}^{r} \frac{\partial h_{\mathrm{air}}^{r}}{\partial \rho_{m}} \mathbf{N}^{eh-} \cdot n \, d\Gamma \\ &+ \int_{\Gamma_{o}} \mathbf{N}^{T} v_{m}^{r} \left(h_{m}^{r} + \frac{1}{2}\left(v_{m}^{r}\right)^{2}\right) \mathbf{N}^{eh} \cdot n \, d\Gamma + \int_{\Gamma_{o}} \mathbf{N}^{T} \rho_{m}^{r} v_{m}^{r} \frac{\partial h_{m}^{r}}{\partial \rho_{m}} \mathbf{N}^{eh} \cdot n \, d\Gamma\end{aligned} \tag{C.27}$$

$$\mathbf{C}_{31} = \int_{\Omega} \mathbf{N}^T \rho_m^r v_m^r \mathbf{N} d\Omega \tag{C.28}$$

$$\mathbf{C}_{32} = -\int_{\Omega} \mathbf{N}^T \mathbf{N} d\Omega \tag{C.29}$$

$$\mathbf{C}_{33} = \int_{\Omega} \mathbf{N}^T h_m^r \mathbf{N} d\Omega + \int_{\Omega} \frac{1}{2} \mathbf{N}^T \left(v_m^r\right)^2 \mathbf{N} d\Omega + \int_{\Omega} \mathbf{N}^T \frac{\partial h_m^r}{\partial \rho_m} \rho_m^r \mathbf{N} d\Omega \tag{C.30}$$

$$\mathbf{C}_{34} = \int_{\Omega} \mathbf{N}^T h_m^r \mathbf{N}^{eh} d\Omega + \int_{\Omega} \frac{1}{2} \mathbf{N}^T \left(v_m^r\right)^2 \mathbf{N}^{eh} d\Omega + \int_{\Omega} \mathbf{N}^T \frac{\partial h_m^r}{\partial \rho_m} \rho_m^r \mathbf{N}^{eh} d\Omega \tag{C.31}$$

$$\mathbf{K}_{31}^0 = -\int_{\Omega} \mathbf{B}^T \rho_m^r \left(h_m^r + \frac{1}{2}\left(v_m^r\right)^2 \right) \mathbf{N} d\Omega - \int_{\Omega} \mathbf{N}^T \rho_m^r \mathbf{N} g \sin\theta d\Omega \tag{C.32}$$

$$\mathbf{K}_{33}^0 = \int_{\Omega} \mathbf{N}^T \frac{\partial h_m^r}{\partial \rho_m} \dot{\rho}_m^r \mathbf{N} d\Omega \tag{C.33}$$

$$\mathbf{K}_{34}^0 = \int_{\Omega} \mathbf{N}^T \frac{\partial h_m^r}{\partial \rho_m} \dot{\rho}_m^r \mathbf{N}^{eh} d\Omega \tag{C.34}$$

$$\mathbf{C}_{31}^0 = \int_{\Omega} \mathbf{N}^T \rho_m^r v_m^r \mathbf{N} d\Omega \tag{C.35}$$

$$\mathbf{C}_{32}^0 = -\int_{\Omega} \mathbf{N}^T \mathbf{N} d\Omega \tag{C.36}$$

$$\mathbf{C}_{33}^0 = \int_{\Omega} \mathbf{N}^T h_m^r \mathbf{N} d\Omega + \int_{\Omega} \frac{1}{2} \mathbf{N}^T \left(v_m^r\right)^2 \mathbf{N} d\Omega \tag{C.37}$$

$$\mathbf{C}_{34}^0 = \int_{\Omega} \mathbf{N}^T h_m^r \mathbf{N}^{eh} d\Omega + \int_{\Omega} \frac{1}{2} \mathbf{N}^T \left(v_m^r\right)^2 \mathbf{N}^{eh} d\Omega \tag{C.38}$$

$$\begin{aligned} \mathbf{f}_3 = & -\int_{\Omega} \mathbf{N}^T \frac{1}{\pi r_i^2} Q^r d\Omega - \int_{\Gamma_d} \mathbf{N}^T \rho_{\mathrm{co}_2}^r v_m^r \left(h_{\mathrm{co}_2}^r + \frac{1}{2}\left(v_m^r\right)^2 \right) \cdot n \, d\Gamma \\ & + \int_{\Gamma_d} \mathbf{N}^T \rho_{\mathrm{air}}^r v_m^r \left(h_{\mathrm{air}}^r + \frac{1}{2}\left(v_m^r\right)^2 \right) \cdot n \, d\Gamma - \int_{\Gamma_o} \mathbf{N}^T \rho_m^r v_m^r \left(h_m^r + \frac{1}{2}\left(v_m^r\right)^2 \right) \cdot n \, d\Gamma \\ & - \int_{\Gamma_q} \mathbf{N}^T \hat{q}_e d\Gamma \end{aligned} \tag{C.39}$$

$$\mathbf{K}_{41}=\int_{\Omega}\left(\mathbf{N}^{eh}\right)^{T}v_m^r\dot{\rho}_m^r\mathbf{N}d\Omega+\int_{\Omega}\left(\mathbf{N}^{eh}\right)^{T}\rho_m^r\dot{v}_m^r\mathbf{N}d\Omega-\int_{\Omega}\left(\mathbf{B}^{eh}\right)^{T}\rho_m^r\left(v_m^r\right)^2\mathbf{N}d\Omega$$
$$-\int_{\Omega}\left(\mathbf{B}^{eh}\right)^{T}\rho_m^r\left(h_m^r+\frac{1}{2}\left(v_m^r\right)^2\right)\mathbf{N}d\Omega-\int_{\Omega}\left(\mathbf{N}^{eh}\right)^{T}\rho_m^r\mathbf{N}g\sin\theta d\Omega$$
$$+\int_{\Gamma_d}\left(\mathbf{N}^{eh}\right)^{T}\rho_{\mathrm{co}_2}^r\left(h_{\mathrm{co}_2}^r+\frac{1}{2}\left(v_m^r\right)^2\right)\mathbf{N}\cdot n\,d\Gamma+\int_{\Gamma_d}\left(\mathbf{N}^{eh}\right)^{T}\rho_{\mathrm{co}_2}^r\left(v_m^r\right)^2\mathbf{N}\cdot n\,d\Gamma \tag{C.40}$$
$$-\int_{\Gamma_d}\left(\mathbf{N}^{eh}\right)^{T}\rho_{\mathrm{air}}^r\left(h_{\mathrm{air}}^r+\frac{1}{2}\left(v_m^r\right)^2\right)\mathbf{N}\cdot n\,d\Gamma-\int_{\Gamma_d}\left(\mathbf{N}^{eh}\right)^{T}\rho_{\mathrm{air}}^r\left(v_m^r\right)^2\mathbf{N}\cdot n\,d\Gamma$$
$$+\int_{\Gamma_o}\left(\mathbf{N}^{eh}\right)^{T}\rho_m^r\left(h_m^r+\frac{1}{2}\left(v_m^r\right)^2\right)\mathbf{N}\cdot n\,d\Gamma+\int_{\Gamma_o}\left(\mathbf{N}^{eh}\right)^{T}\rho_m^r\left(v_m^r\right)^2\mathbf{N}\cdot n\,d\Gamma$$

$$\mathbf{K}_{42}=\int_{\Omega}\left(\mathbf{N}^{eh}\right)^{T}\frac{\partial h_m^r}{\partial p}\dot{\rho}_m^r\mathbf{N}d\Omega+\int_{\Omega}\left(\mathbf{N}^{eh}\right)^{T}\frac{\partial^2 h_m^r}{\partial p^2}\dot{p}^r\rho_m^r\mathbf{N}d\Omega$$
$$+\int_{\Omega}\left(\mathbf{N}^{eh}\right)^{T}\frac{\partial^2 h_m^r}{\partial p\partial\rho_m}\dot{\rho}_m^r\rho_m^r\mathbf{N}d\Omega-\int_{\Omega}\left(\mathbf{B}^{eh}\right)^{T}\rho_m^r\frac{\partial h_m^r}{\partial p}v_m^r\mathbf{N}d\Omega$$
$$+\int_{\Omega}\left(\mathbf{N}^{eh}\right)^{T}\frac{1}{\pi r_i^2}\frac{dQ^r}{dT}\frac{\partial T^r}{\partial p}\mathbf{N}d\Omega+\int_{\Gamma_d}\left(\mathbf{N}^{eh}\right)^{T}\rho_{\mathrm{co}_2}^r v_m^r\frac{\partial h_{\mathrm{co}_2}^r}{\partial p}\mathbf{N}\cdot n\,d\Gamma \tag{C.41}$$
$$-\int_{\Gamma_d}\left(\mathbf{N}^{eh}\right)^{T}\rho_{\mathrm{air}}^r v_m^r\frac{\partial h_{\mathrm{air}}^r}{\partial p}\mathbf{N}\cdot n\,d\Gamma+\int_{\Gamma_o}\left(\mathbf{N}^{eh}\right)^{T}\rho_m^r v_m^r\frac{\partial h_m^r}{\partial p}\mathbf{N}\cdot n\,d\Gamma$$

$$\mathbf{K}_{43}=\int_{\Omega}\left(\mathbf{N}^{eh}\right)^{T}\frac{\partial h_m^r}{\partial\rho_m}\dot{\rho}_m^r\mathbf{N}d\Omega+\int_{\Omega}\left(\mathbf{N}^{eh}\right)^{T}\frac{\partial^2 h_m^r}{\partial p\partial\rho_m}\dot{p}^r\rho_m^r\mathbf{N}d\Omega+\int_{\Omega}\left(\mathbf{N}^{eh}\right)^{T}\frac{\partial h_m^r}{\partial p}\dot{p}^r\mathbf{N}d\Omega$$
$$+\int_{\Omega}\left(\mathbf{N}^{eh}\right)^{T}\frac{\partial^2 h_m^r}{\partial\rho_m^2}\dot{\rho}_m^r\rho_m^r\mathbf{N}d\Omega-\int_{\Omega}\left(\mathbf{N}^{eh}\right)^{T}v_m^r\mathbf{N}g\sin\theta d\Omega+\int_{\Omega}\left(\mathbf{N}^{eh}\right)^{T}\frac{\partial h_m^r}{\partial\rho_m}\dot{\rho}_m^r\mathbf{N}d\Omega$$
$$+\int_{\Omega}\left(\mathbf{N}^{eh}\right)^{T}v_m^r\dot{v}_m^r\mathbf{N}d\Omega-\int_{\Omega}\left(\mathbf{B}^{eh}\right)^{T}\left(h_m^r+\frac{1}{2}\left(v_m^r\right)^2\right)v_m^r\mathbf{N}d\Omega-\int_{\Omega}\left(\mathbf{B}^{eh}\right)^{T}\rho_m^r\frac{\partial h_m^r}{\partial\rho_m}v_m^r\mathbf{N}d\Omega$$
$$+\int_{\Omega}\left(\mathbf{N}^{eh}\right)^{T}\frac{1}{\pi r_i^2}\frac{dQ^r}{dT}\frac{\partial T^r}{\partial\rho_m}\mathbf{N}d\Omega+\int_{\Gamma_d}\left(\mathbf{N}^{eh}\right)^{T}v_m^r\left(h_{\mathrm{co}_2}^r+\frac{1}{2}\left(v_m^r\right)^2\right)\mathbf{N}\cdot n\,d\Gamma \tag{C.42}$$
$$+\int_{\Gamma_d}\left(\mathbf{N}^{eh}\right)^{T}\rho_{\mathrm{co}_2}^r v_m^r\frac{\partial h_{\mathrm{co}_2}^r}{\partial\rho_m}\mathbf{N}\cdot n\,d\Gamma-\int_{\Gamma_d}\left(\mathbf{N}^{eh}\right)^{T}v_m^r\left(h_{\mathrm{air}}^r+\frac{1}{2}\left(v_m^r\right)^2\right)\mathbf{N}\cdot n\,d\Gamma$$
$$-\int_{\Gamma_d}\left(\mathbf{N}^{eh}\right)^{T}\rho_{\mathrm{air}}^r v_m^r\frac{\partial h_{\mathrm{air}}^r}{\partial\rho_m}\mathbf{N}\cdot n\,d\Gamma+\int_{\Gamma_o}\left(\mathbf{N}^{eh}\right)^{T}v_m^r\left(h_m^r+\frac{1}{2}\left(v_m^r\right)^2\right)\mathbf{N}\cdot n\,d\Gamma$$
$$+\int_{\Gamma_o}\left(\mathbf{N}^{eh}\right)^{T}\rho_m^r v_m^r\frac{\partial h_m^r}{\partial\rho_m}\mathbf{N}\cdot n\,d\Gamma$$

$$\mathbf{K}_{44}=\int_{\Omega}\left(\mathbf{N}^{eh}\right)^{T}\frac{\partial h_m^r}{\partial \rho_m}\dot{\rho}_m^r\mathbf{N}^{eh}d\Omega+\int_{\Omega}\left(\mathbf{N}^{eh}\right)^{T}\frac{\partial^2 h_m^r}{\partial p\partial \rho_m}\dot{p}^r\rho_m^r\mathbf{N}^{eh}d\Omega$$
$$+\int_{\Omega}\left(\mathbf{N}^{eh}\right)^{T}\frac{\partial h_m^r}{\partial p}\dot{p}^r\mathbf{N}^{eh}d\Omega+\int_{\Omega}\left(\mathbf{N}^{eh}\right)^{T}\frac{\partial^2 h_m^r}{\partial \rho_m^2}\dot{\rho}_m^r\rho_m^r\mathbf{N}^{eh}d\Omega$$
$$-\int_{\Omega}\left(\mathbf{N}^{eh}\right)^{T}v_m^r\mathbf{N}^{eh}g\sin\theta d\Omega+\int_{\Omega}\left(\mathbf{N}^{eh}\right)^{T}\frac{\partial h_m^r}{\partial \rho_m}\dot{\rho}_m^r\mathbf{N}^{eh}d\Omega$$
$$+\int_{\Omega}\left(\mathbf{N}^{eh}\right)^{T}v_m^r\dot{v}_m^r\mathbf{N}^{eh}d\Omega-\int_{\Omega}\left(\mathbf{B}^{eh}\right)^{T}\left(h_m^r+\frac{1}{2}\left(v_m^r\right)^2\right)v_m^r\mathbf{N}^{eh}d\Omega$$
$$-\int_{\Omega}\left(\mathbf{B}^{eh}\right)^{T}\rho_m^r\frac{\partial h_m^r}{\partial \rho_m}v_m^r\mathbf{N}^{eh}d\Omega+\int_{\Omega}\left(\mathbf{N}^{eh}\right)^{T}\frac{1}{\pi r_i^2}\frac{dQ^r}{dT}\frac{\partial T^r}{\partial \rho_m}\mathbf{N}^{eh}d\Omega$$
$$+\int_{\Gamma_d}\left(\mathbf{N}^{eh}\right)^{T}v_m^r\left(h_{\mathrm{co}_2}^r+\frac{1}{2}\left(v_m^r\right)^2\right)\mathbf{N}^{eh+}\cdot n\,d\Gamma+\int_{\Gamma_d}\left(\mathbf{N}^{eh}\right)^{T}\rho_{\mathrm{co}_2}^r v_m^r\frac{\partial h_{\mathrm{co}_2}^r}{\partial \rho_m}\mathbf{N}^{eh+}\cdot n\,d\Gamma$$
$$-\int_{\Gamma_d}\left(\mathbf{N}^{eh}\right)^{T}v_m^r\left(h_{\mathrm{air}}^r+\frac{1}{2}\left(v_m^r\right)^2\right)\mathbf{N}^{eh-}\cdot n\,d\Gamma-\int_{\Gamma_d}\left(\mathbf{N}^{eh}\right)^{T}\rho_{\mathrm{air}}^r v_m^r\frac{\partial h_{\mathrm{air}}^r}{\partial \rho_m}\mathbf{N}^{eh-}\cdot n\,d\Gamma$$
$$+\int_{\Gamma_o}\left(\mathbf{N}^{eh}\right)^{T}v_m^r\left(h_m^r+\frac{1}{2}\left(v_m^r\right)^2\right)\mathbf{N}^{eh}\cdot n\,d\Gamma+\int_{\Gamma_o}\left(\mathbf{N}^{eh}\right)^{T}\rho_m^r v_m^r\frac{\partial h_m^r}{\partial \rho_m}\mathbf{N}^{eh}\cdot n\,d\Gamma \tag{C.43}$$

$$\mathbf{C}_{41}=\int_{\Omega}\left(\mathbf{N}^{eh}\right)^{T}\rho_m^r v_m^r\mathbf{N}d\Omega \tag{C.44}$$

$$\mathbf{C}_{42}=-\int_{\Omega}\left(\mathbf{N}^{eh}\right)^{T}\mathbf{N}d\Omega \tag{C.45}$$

$$\mathbf{C}_{43}=\int_{\Omega}\left(\mathbf{N}^{eh}\right)^{T}h_m^r\mathbf{N}d\Omega+\int_{\Omega}\frac{1}{2}\left(\mathbf{N}^{eh}\right)^{T}\left(v_m^r\right)^2\mathbf{N}d\Omega+\int_{\Omega}\left(\mathbf{N}^{eh}\right)^{T}\frac{\partial h_m^r}{\partial \rho_m}\rho_m^r\mathbf{N}d\Omega \tag{C.46}$$

$$\mathbf{C}_{44}=\int_{\Omega}\left(\mathbf{N}^{eh}\right)^{T}h_m^r\mathbf{N}^{eh}d\Omega+\int_{\Omega}\frac{1}{2}\left(\mathbf{N}^{eh}\right)^{T}\left(v_m^r\right)^2\mathbf{N}^{eh}d\Omega+\int_{\Omega}\left(\mathbf{N}^{eh}\right)^{T}\frac{\partial h_m^r}{\partial \rho_m}\rho_m^r\mathbf{N}^{eh}d\Omega \tag{C.47}$$

$$\mathbf{K}_{41}^{0}=-\int_{\Omega}\left(\mathbf{B}^{eh}\right)^{T}\rho_m^r\left(h_m^r+\frac{1}{2}\left(v_m^r\right)^2\right)\mathbf{N}d\Omega-\int_{\Omega}\left(\mathbf{N}^{eh}\right)^{T}\rho_m^r\mathbf{N}g\sin\theta d\Omega \tag{C.48}$$

$$\mathbf{K}_{43}^{0}=\int_{\Omega}\left(\mathbf{N}^{eh}\right)^{T}\frac{\partial h_m^r}{\partial \rho_m}\dot{\rho}_m^r\mathbf{N}d\Omega \tag{C.49}$$

$$\mathbf{K}_{44}^{0}=\int_{\Omega}\left(\mathbf{N}^{eh}\right)^{T}\frac{\partial h_m^r}{\partial \rho_m}\dot{\rho}_m^r\mathbf{N}^{eh}d\Omega \tag{C.50}$$

$$\mathbf{C}_{41}^{0}=\int_{\Omega}\left(\mathbf{N}^{eh}\right)^{T}\rho_m^r v_m^r\mathbf{N}d\Omega \tag{C.51}$$

$$\mathbf{C}_{42}^{0}=-\int_{\Omega}\left(\mathbf{N}^{eh}\right)^{T}\mathbf{N}d\Omega \tag{C.52}$$

$$\mathbf{C}_{43}^{0}=\int_{\Omega}\left(\mathbf{N}^{eh}\right)^{T}h_m^r\mathbf{N}d\Omega+\int_{\Omega}\frac{1}{2}\left(\mathbf{N}^{eh}\right)^{T}\left(v_m^r\right)^2\mathbf{N}d\Omega \tag{C.53}$$

$$\mathbf{C}_{44}^{0} = \int_{\Omega} \left(\mathbf{N}^{eh}\right)^{T} h_m^r \mathbf{N}^{eh} d\Omega + \int_{\Omega} \frac{1}{2} \left(\mathbf{N}^{eh}\right)^{T} \left(v_m^r\right)^2 \mathbf{N}^{eh} d\Omega \tag{C.54}$$

$$\begin{aligned} \mathbf{f}_4 = & -\int_{\Omega} \left(\mathbf{N}^{eh}\right)^{T} \frac{1}{\pi r_i^2} Q^r d\Omega - \int_{\Gamma_d} \left(\mathbf{N}^{eh+}\right)^{T} \rho_{\mathrm{co}_2}^r v_m^r \left(h_{\mathrm{co}_2}^r + \frac{1}{2}\left(v_m^r\right)^2\right) \cdot n \, d\Gamma \\ & + \int_{\Gamma_d} \left(\mathbf{N}^{eh-}\right)^{T} \rho_{\mathrm{air}}^r v_m^r \left(h_{\mathrm{air}}^r + \frac{1}{2}\left(v_m^r\right)^2\right) \cdot n \, d\Gamma - \int_{\Gamma_o} \left(\mathbf{N}^{eh}\right)^{T} \rho_m^r v_m^r \left(h_m^r + \frac{1}{2}\left(v_m^r\right)^2\right) \cdot n \, d\Gamma \\ & - \int_{\Gamma_q} \left(\mathbf{N}^{eh}\right)^{T} \hat{q}_e d\Gamma \end{aligned} \tag{C.55}$$

References

1. Brill, J.P. and H. Mukherjee, *Multiphase flow in wells*. 1999: Richardson, Tex.: Henry L. Doherty Memorial Fund of AIME, Society of Petroleum Engineers.
2. Hasan, A.R., C.S. Kabir, and C. Sarica, *Fluid flow and heat transfer in wellbores*. 2002: Society of Petroleum Engineers Richardson, TX.
3. Freeston, D. and T. Hadgu. *Comparison of results from some wellbore simulators using a data bank*. in *Proceedings of the 10th Geothermal Workshop, New Zealand*. 1988.
4. Probst, A., C. Gunn, and G. Andersen. *A preliminary comparison of pressure drop models used in simulating geothermal production wells*. in *14th New Zealand Geothermal Workshop*. 1992. Auckland University.
5. Faghri, A. and Y. Zhang, *Transport phenomena in multiphase systems*. 2006: Academic Press.
6. Stone, T., N. Edmunds, and B. Kristoff. *A comprehensive wellbore/reservoir simulator*. in *SPE Symposium on Reservoir Simulation*. 1989.
7. Hadgu, T., R.W. Zimmerman, and G.S. Bodvarsson, *Coupled reservoir-wellbore simulation of geothermal reservoir behavior.* Geothermics, 1995. **24**(2): p. 145-166.
8. Livescu, S., et al., *A fully-coupled thermal multiphase wellbore flow model for use in reservoir simulation.* Journal of Petroleum Science and Engineering, 2010. **71**(3–4): p. 138-146.
9. Hasan, A.R. and C.S. Kabir, *Modeling two-phase fluid and heat flows in geothermal wells.* Journal of Petroleum Science and Engineering, 2010. **71**(1–2): p. 77-86.
10. Pan, L. and C.M. Oldenburg, *Rigorous process simulation of compressed air energy storage (CAES) in porous media systems*, in *Computational Models for CO2 Geo-sequestration & Compressed Air Energy Storage*, R. Al-Khoury and J. Bundschuh, Editors. 2014, CRC Press. p. 574.
11. Cronshaw, M. and J. Bolling. *A numerical model of the non-isothermal flow of carbon dioxide in wellbores*. in *SPE California Regional Meeting*. 1982.
12. Lu, M. and L.D. Connell, *Non-isothermal flow of carbon dioxide in injection wells during geological storage.* International Journal of Greenhouse Gas Control, 2008. **2**(2): p. 248-258.
13. Lindeberg, E., *Modelling pressure and temperature profile in a CO2 injection well.* Energy Procedia, 2011. **4**(0): p. 3935-3941.
14. Paterson, L., et al. *Numerical modeling of pressure and temperature profiles including phase transitions in carbon dioxide wells*. in *SPE Annual Technical Conference and Exhibition*. 2008.
15. Pan, L., et al., *Wellbore flow model for carbon dioxide and brine.* Energy Procedia, 2009. **1**(1): p. 71-78.
16. Remoroza, A.I., B. Moghtaderi, and E. Doroodchi. *Coupled wellbore and 3d reservoir simulation of a co2 egs*. in *Proceedings, SGP-TR-191, 36th Workshop on Geothermal Reservoir Engineering, Stanford University, Stanford, California*. 2011.
17. Shi, H., et al., *Drift-flux modeling of two-phase flow in wellbores.* Spe Journal, 2005. **10**(1): p. 24-33.
18. Ishii, M. and T. Hibiki, *Thermo-fluid dynamics of two-phase flow. 2006: Springer Science*. 2006, IN, USA: Springer.
19. Musivand Arzanfudi, M. and R. Al-Khoury, *On the theory of CO2 geo-sequestration*, in *Computational Models for CO2 Geo-sequestration & Compressed Air Energy Storage*, R. Al-Khoury and J. Bundschuh, Editors. 2014, CRC Press. p. 11-77.
20. Rehm, R.G. and H.R. Baum, *The Equations of Motion for Thermally Driven, Buoyant Flows.* J. Res. Bur. Stand., 1978. **83**(3): p. 297-308.

21. Paolucci, S., *On the Filtering of Sound from the Navier–Stokes Equations*. 1982: Albuquerque, NM.
22. Principe, J. and R. Codina, *Mathematical models for thermally coupled low speed flows.* Advances in Theoretical and Applied Mechanics, 2009. **2**: p. 93-112.
23. Reddy, J.N. and D.K. Gartling, *The finite element method in heat transfer and fluid dynamics*. Third ed. 2010, Boca Raton, FL: CRC press.
24. Cho, M.H., H.G. Choi, and J.Y. Yoo, *A direct reinitialization approach of level-set/splitting finite element method for simulating incompressible two-phase flows.* International Journal for Numerical Methods in Fluids, 2010: p. n/a-n/a.
25. Zi, G. and T. Belytschko, *New crack-tip elements for XFEM and applications to cohesive cracks.* Int. J. Numer. Meth. Engng, 2003. **57**: p. 2221-2240.
26. Fries, T.-P. and T. Belytschko, *The extended/generalized finite element method: An overview of the method and its applications.* International Journal for Numerical Methods in Engineering, 2010. **84**(3): p. 253-304.
27. Al-Khoury, R., T. Kölbel, and R. Schramedei, *Efficient numerical modeling of borehole heat exchangers.* Computers & Geosciences, 2010. **36**(10): p. 1301-1315.
28. Pan, L., S.W. Webb, and C.M. Oldenburg, *Analytical solution for two-phase flow in a wellbore using the drift-flux model.* Advances in Water Resources, 2011. **34**(12): p. 1656-1665.
29. Redlich, O. and J.N.S. Kwong, *On the Thermodynamics of Solutions. V. An Equation of State. Fugacities of Gaseous Solutions.* Chemical Reviews, 1949. **44**(1): p. 233-244.
30. Spycher, N., K. Pruess, and J. Ennis-King, *CO_2-H_2O mixtures in the geological sequestration of CO_2. I. Assessment and calculation of mutual solubilities from 12 to 100°C and up to 600 bar.* Geochim. Cosmochim. Acta, 2003. **67**(16): p. 3015-3031.
31. Span, R. and W. Wagner, *A new equation of state for carbon dioxide covering the fluid region from the triple-point temperature to 1100 K at pressures up to 800 MPa.* J. Phys. Chem. Ref. Data, 1996. **25**(6): p. 1509-1596.
32. Fenghour, A., W.A. Wakeham, and V. Vesovic, *The viscosity of carbon dioxide.* J. Phys. Chem. Ref. Data, 1998. **27**(1): p. 31-44.
33. Rathakrishnan, E., *Fluid Mechanics : An Introduction*. Third ed. 2012, New Delhi: PHI.